ARTICLES
https://doi.org/10.1038/s41561-021-00784-3
nature geoscience

Check for updates

OPEN

Possible link between Earth's rotation rate and oxygenation

J. M. Klatt[1,2,5]✉, A. Chennu[1,3,5], B. K. Arbic[2], B. A. Biddanda[4] and G. J. Dick[2]✉

The biotic and abiotic controls on major shifts in atmospheric oxygen and the persistence of low-oxygen periods over a majority of Earth's history remain under debate. Explanations of Earth's stepwise pattern of oxygenation have mostly neglected the effect of changing diel illumination dynamics linked to daylength, which has increased through geological time due to Earth's rotational deceleration caused by tidal friction. Here we used microsensor measurements and dynamic modelling of interfacial solute fluxes in cyanobacterial mats to investigate the effect of changing daylength on Precambrian benthic ecosystems. Simulated increases in daylength across Earth's historical range boosted the diel benthic oxygen export, even when the gross photosynthetic production remained constant. This fundamental relationship between net productivity and daylength emerges from the interaction of diffusive mass transfer and diel illumination dynamics, and is amplified by metabolic regulation and microbial behaviour. We found that the resultant daylength-driven surplus organic carbon burial could have shaped the increase in atmospheric oxygen that occurred during the Great and Neoproterozoic Oxidation Events. Our suggested mechanism, which links the coinciding increases in daylength and atmospheric oxygen via enhanced net productivity, reveals a possible contribution of planetary mechanics to the evolution of Earth's biology and geochemistry.

The rise of free oxygen (O_2) in the Earth's atmosphere and oceans enabled the evolution of aerobic life[1]. Oxygenic photosynthesis (OP) in microbial mats was a substantial source of O_2 for the Great Oxidation Event (GOE) ~2.4 billion years ago (Ga), during the stable low-O_2 conditions that followed and for the Neoproterozoic Oxygenation Event (NOE) ~600 Ma (ref. [2]). The biological[3,4], tectonic[5] and geochemical[6,7] mechanisms that determined this stepwise pattern of oxygenation are still debated. Here we explore a previously unconsidered link between Earth's oxygenation pattern and rotation rate, which decelerated over geological time due to tidal friction[8,9]. We establish a mechanistic link between daylength and export fluxes of solutes from microbial mats. Experimental measurements and models of Proterozoic cyanobacterial mat analogues show that longer daylength increases benthic O_2 export, changes the balance between aerobic and anaerobic remineralization, and thus enhances the diel organic carbon (C_{org}) burial. We then investigated the remarkable similarity between the timing and pattern of increase in atmospheric O_2 (pO_2 as a fraction of the present atmospheric level (PAL)) and daylength. We found that increases in daylength could plausibly have influenced Earth's oxygenation, particularly around key oxidation events, and thus helped to pave the way for the evolution of plants and animals of the modern world.

Longer days increase net benthic O_2 export fluxes

Earth's rotation period is 24 hours at present, but may have been as low as 6 hours at ages older than 4 Ga (refs [8,10,11]). Thus, daylength (that is, one rotational or diel period) and the illumination period may have increased more than threefold since the evolutionary origin of photosynthesis. This implies that the dynamics of illumination (rate of increase and decrease) within the diel period changed substantially. The rate of gross photosynthetic production (GPP) is governed by the instantaneous photon flux, irrespective of illumination dynamics and daylength. The net production rate, equivalent to diel C_{org} burial, is the result of this GPP and the rate of C_{org} consumption. As opposed to GPP, the net production of benthic ecosystems is expected to be influenced by changes in the illumination dynamics. In such systems, rates of net productivity are not only shaped by the instantaneous photon flux, but also by fluxes of metabolic substrates and products, which are governed by molecular diffusion. Thus, import, export and accumulation of metabolites should be sensitive to daylength due to the interaction between illumination dynamics and diffusive mass transfer.

We developed a modelled understanding of this interaction and first explored the implications for the export fluxes of the photosynthetic product O_2. Our modelling framework[12] formulates benthic ecosystems as diffusive–reactive systems with OP, anoxygenic photosynthesis (AP), aerobic respiration (R_{aero}), sulfate reduction (anaerobic respiration (R_{anaero})) and abiotic sulfide oxidation (SOX) (Extended Data Fig. 1 and Supplementary Video 1). Starting with a simple in silico mat with only OP and R_{aero}, simulations with the same rate of GPP showed that longer days yield higher export fluxes, that is, an increase in O_2 escape to the overlying water (Fig. 1a,b). The mechanism behind this relationship is apparent in the duration between the maxima of gross O_2 production and export (Fig. 1a), which illustrates how mass transfer resistance delays the O_2 escape. The export-limiting delay represents a smaller fraction of the day for longer daylengths. Longer days build up steeper O_2 gradients and therefore higher fluxes, both upward and downward (Extended Data Fig. 2a). In thin mats, the latter would interact with the mat substrate (for example, pyrite), and possibly create a daylength-driven increase in preserved weathering signals[13]. The daylength-driven increase in O_2 fluxes also alters the availability of O_2 within the mat, boosts the fraction of produced

[1]Microsensor Group, Max Planck Institute for Marine Microbiology, Bremen, Germany. [2]Department of Earth & Environmental Sciences, University of Michigan, Ann Arbor, MI, USA. [3]Data Science and Technology, Leibniz Centre for Tropical Marine Research, Bremen, Germany. [4]Annis Water Resources Institute, Grand Valley State University, Muskegon, MI, USA. [5]These authors contributed equally: J. M. Klatt, A. Chennu. ✉e-mail: jklatt@mpi-bremen.de; gdick@umich.edu

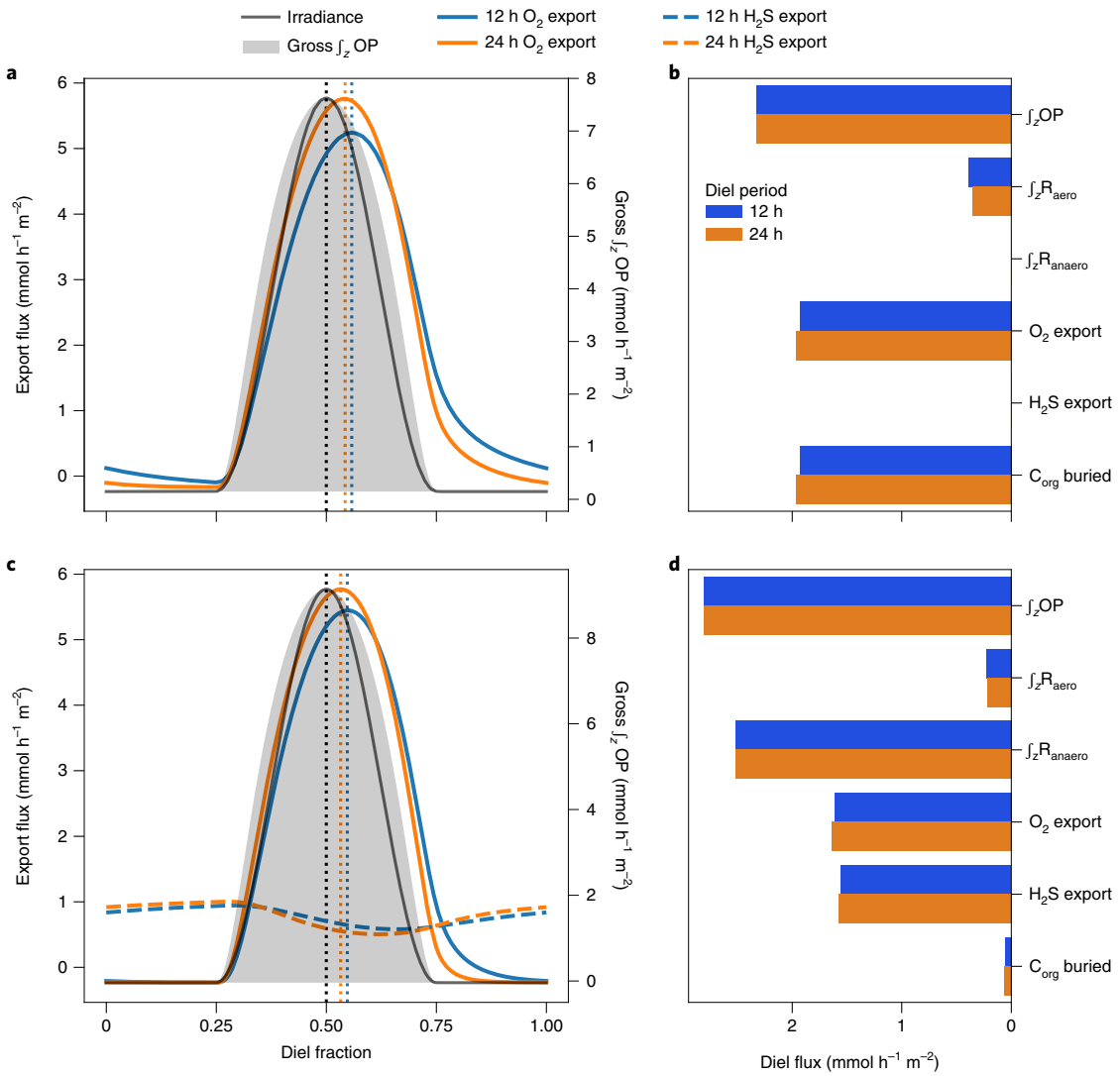

Fig. 1 | Modelled temporal evolution of gross O_2 production, O_2 and H_2S export, and diel averages for C_{org} respiration and burial compared for 12 h versus 24 h daylengths. a, Depth-integrated gross OP ($\int_z$OP, grey fill) in a pure OP system ('OP no H_2S') under a water column with 25 µM O_2 ($pO_2 = 0.1$) is identical for the two daylengths with the time of day viewed as a fraction of the diel period. However, the diel fraction during which export is tempered by mass transfer, illustrated by the duration between the maxima of photosynthesis (black dotted line) and export (blue and orange dotted lines), is sensitive to daylength. **b**, As longer days export more O_2, less O_2 is available for aerobic respiration ($\int_z R_{aero}$) in the mat, and therefore the burial of C_{org} increases with daylength. **c**, In the presence of anaerobic respiration by sulfur-reducing bacteria, both O_2 and H_2S export fluxes are modulated by daylength, even though the gross photosynthesis and sulfide production by anaerobic respiration are independent of the illumination dynamics in this simulation ('OP SRB constant'). **d**, The diel C_{org} burial flux is defined here as the photosynthetically produced C_{org} that escapes both aerobic and anaerobic respiration ($\int_z OP - \int_z R_{aero} - \int_z R_{anaero}$) and equals the difference between the export budgets of O_2 and H_2S (shown in C_{org} equivalents). The decrease of $\int_z R_{aero}$ compared with the diel budget in **b** is due to abiotic sulfide oxidation (SOX), an alternative sink of O_2. As $\int_z R_{anaero}$ is set to be constant, the overall effect remains: mats export more O_2 and retain more C_{org} in longer days.

C_{org} that escapes R_{aero} and thus decreases remineralization efficiency (Fig. 1b). Consequently, daylength interacts with the net productivity of benthic systems, which relates to the short-term (that is, diel) C_{org} excess, and possibly the long-term C_{org} burial rate, a crucial determinant for the state of global pO_2 (refs [1,14]). Overall, although GPP rates are unaffected by changes in daylength, C_{org} burial is modulated through the physics of molecular diffusion.

Daylength increases O_2 export more than reductant export

A more realistic scenario includes R_{anaero} as an additional sink of C_{org}, which we implemented in the form of sulfate reduction. Conceptually, sulfate and sulfide, the substrate and product, respectively, can be exchanged with any other redox couple, such as Fe(III)/Fe(II). We focus on the sulfur cycle because of the early evolutionary onset of sulfate reduction[15] and because sulfide was transiently abundant in Precambrian coastal habitats[16]. We first chose a mat scenario with the R_{anaero} rate fixed to a constant value, to isolate the effect of daylength on diffusion-driven dynamics of sulfide export (Fig. 1c). Like O_2 fluxes, the reductant export fluxes are shaped by molecular diffusion and rates of production and consumption within the mat (R_{anaero} and SOX). The latter is an additional sink of O_2 and is thus competitive with R_{aero}. Consequently, the C_{org} that escapes both anaerobic and aerobic remineralization can be represented as the difference between the O_2 and H_2S export fluxes (Fig. 1c,d and Extended Data Fig. 1). As both fluxes increase with daylength, the rates of SOX decrease. Owing to this moderating

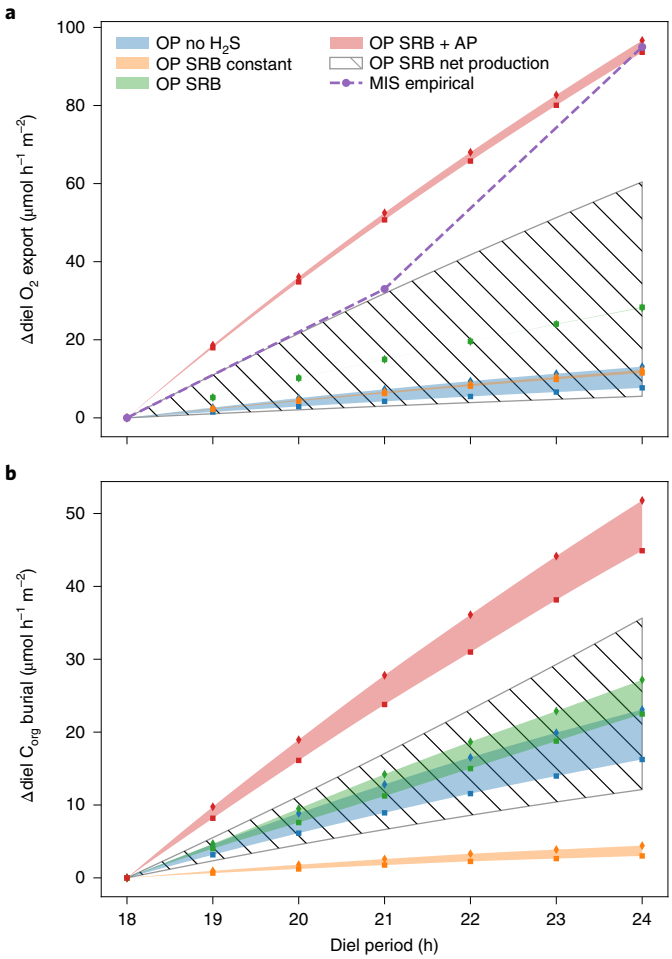

Fig. 2 | Daylength dependence of benthic diel O_2 export and C_{org} burial fluxes under various metabolic and boundary conditions. The effect of daylength is explored for mats with different metabolic repertoires across a range of O_2 boundary conditions (0–1 pO_2 in the shaded areas; Extended Data Figs. 3 and 5). **a**, O_2 export fluxes consistently increase across all the metabolic scenarios and boundary conditions. Measured O_2 export from cyanobacterial mats with chemosynthetic competition ('MIS empirical') provides empirical confirmation of the dependency of fluxes on daylength. **b**, Owing to the O_2 export flux modulation, the diel C_{org} burial also consistently increases with daylength despite the counteracting effect of an increasing H_2S export for scenarios with R_{anaero} (Fig. 1). Fluxes are shown relative to the values of each scenario at 18 h, which corresponds to daylength before the GOE. Metabolic scenarios explored were: purely aerobic systems with only OP and no R_{anaero} ('OP no H_2S'), systems with constant R_{anaero} that is not affected by changing diel illumination dynamics ('OP SRB constant'), systems with metabolically complex R_{anaero} that responds to local changes in O_2 and sulfide, which are governed by illumination dynamics ('OP SRB') and mat systems with both AP and OP ('OP SRB + AP'). Systems with sulfide-inhibited OP exhibited a steepness of daylength dependency out of scale, and are shown in Extended Data Fig. 8. For the R_{anaero} scenario with a modest inhibition by O_2 and H_2S ('OP SRB'), we additionally explored a wide range of plausible GPP levels ('OP SRB net production'). Notably, the effect of variations in GPP on burial is less pronounced than that on O_2 export.

effect of SOX, R_{aero} is less sensitive to daylength than it is in a reductant-free scenario. The effect of an increased O_2 export on the diel C_{org} burial rate is therefore counteracted, but not overwhelmed, by concomitant increases in H_2S export (Fig. 1d). To further explore if the increase of diel C_{org} burial is maintained when R_{anaero} is affected by local solute dynamics, we implemented sulfate-reducing bacteria (SRB) that are inhibited by O_2 and H_2S, as observed in modern mats[17–19]. Across a range of inhibition strengths, diel C_{org} burial consistently increases with daylength (Fig. 2 and Extended Data Fig. 3).

Given that the Earth's redox landscape changed along with daylength through geological time, we studied the sensitivity of daylength-driven diel C_{org} burial to reductant and O_2 availability in the water column. Diel O_2 export and C_{org} burial fluxes increased with daylength across all O_2 boundary conditions (Fig. 2). Increasing O_2 in the water column had a strong enhancing effect on R_{aero} and negative effect on O_2 export fluxes. For the diel C_{org} burial rate, determined by both R_{aero} and R_{anaero}, the effect of O_2 levels in the water column was variable (Extended Data Fig. 3). Depending on the inhibition strength of O_2 on R_{anaero}, C_{org} burial either increases or decreases with the O_2 boundary conditions. Given that R_{anaero} is O_2 sensitive, the negative impact of pO_2 is overwhelmed by the positive effect of daylength enhancing diel benthic C_{org} burial over Earth's history.

To explore the interactions between reductant availability and C_{org} burial with daylength, we also included AP using H_2S as an electron donor that competes with OP for the contribution to GPP based on mat-intrinsic reductant and light levels[20] (Extended Data Fig. 4). With AP present in mats, the fraction of the day that exports O_2 is reduced for shorter daylengths because of the time required for AP to deplete the local sulfide concentration below the thresholds that allow OP to occur (Extended Data Fig. 5). Although the total GPP (AP + OP) is unaffected by daylength, the fraction of the day during which O_2 is produced decreases markedly with daylength. Concomitantly, R_{anaero} decreases with daylength due to the increasing inhibition by O_2. Although counterintuitive, R_{aero} decreases with daylength because SOX becomes more competitive for O_2 due to the increasing fractions of the day with O_2 production. Consequently, across a range of sulfide and O_2 levels in the overlying water, we found that the C_{org} burial of systems with AP is more steeply modulated by daylength compared with that for communities with only OP (Fig. 2). Interestingly, the dependency of the diel C_{org} burial on the reductant boundary condition was negligible compared to that on daylength. Therefore, the metabolic repertoire, rather than the water column redox conditions, shapes the response of benthic systems to daylength in terms of diel C_{org} burial.

Overall, we show that the net productivity, that is, the short-term C_{org} burial of benthic ecosystems, and thus a crucial determinant of the source strength for global pO_2, can increase with daylength over Earth's age without assuming a decrease in the global O_2 sink strength or an increase in GPP. However, the range of global GPP probably varied substantially, for example, due to new evolutionary avenues of primary production[21], redox and phosphate oscillations related to weathering during the 'boring billion' years[6], continental reconfiguration[22], long-term changes in insolation[23] or even daylength-related changes in ocean circulation and nutrient supply by upwelling[24]. We therefore evaluated the sensitivity of daylength-driven increases in benthic O_2 export to the rates of GPP. As expected, O_2 export displays a steep dependency on GPP, but daylength-driven changes in C_{org} burial are substantially less sensitive to GPP (Fig. 2). This implies that the areal coverage of benthic habitats rather than the evolution of GPP by the inhabitants is of greatest relevance for daylength-driven effects.

Empirical verification of the daylength effect

To reify the concept of export fluxes being modulated by daylength, we measured rates of photosynthesis and O_2 export in cyanobacterial mats from the Middle Island Sinkhole (MIS), an extant analogue of Proterozoic mats under low-O_2 conditions[25]. Net O_2 production consistently occurred only after extended exposure time to light (Fig. 3a). White sulfur-oxidizing bacteria (SOB) atop the mat during night and morning reduced the light availability for photosynthesis[26]. The cyanobacteria exclusively performed AP, and thereby

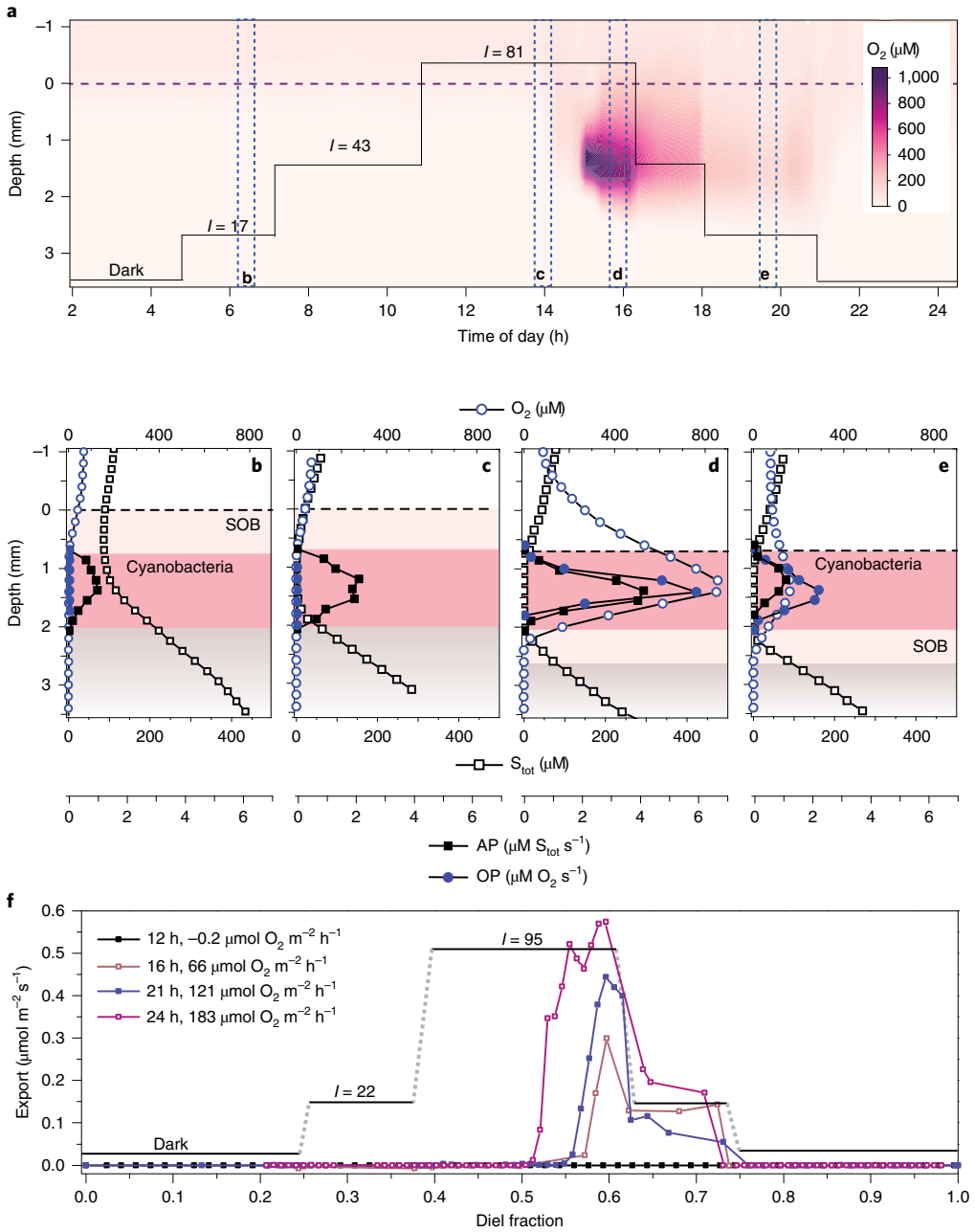

Fig. 3 | Microsensor measurements in freshly collected cores with intact MIS mat samples during the simulated diel periods. a, Vertical profiles of O_2 in one of the mats are shown as a colour-coded map over the simulated diel light cycle and illustrate a delay in the net photosynthetic O_2 production. The light intensity at the mat surface is indicated as *I* (μmol photons m^{-2} s^{-1}). **b**–**e**, Depth profiles of O_2 (open blue circles), total sulfide (calculated from $[H_2S]$ and pH; open black squares), gross OP and sulfide-driven AP (filled blue circles and black squares, respectively) ($n = 3$–4 for measurements at each depth) at the selected time points (**b**–**e**) shown in **a** reveal the cascade of structural and metabolic changes that result in a delayed O_2 release. The vertical mat structure is represented as shaded areas. Although sulfide was depleted by AP upon illumination (**b** and **c**), OP occurred despite extended illumination only when the mat structure changed (**d** and **e**). The resultant delay in net O_2 production was consistently observed in four separate mat samples exposed to similar water-column conditions, and throughout seven additional mat samples exposed to a wide range of sulfide and O_2 levels in the water column (Extended Data Fig. 6). The magnitude of the fluxes and the duration of the delays were dependent on the specific sample and on the water-column redox conditions. **f**, The momentary export flux across the benthic interface was measured over 12–24 h simulated daylengths in one mat sample exposed to 1 μM O_2 from the water column in the absence of sulfide (Extended Data Fig. 7). The resultant diel O_2 export is shown in the key and increased with daylength.

depleted the sulfide underneath the SOB layer (Fig. 3b,c). The sudden onset of O_2 production during the phase of high light in the early afternoon (Fig. 3d) coincided with the downward migration of the light-reflecting white SOB, which was probably induced by depletion of sulfide by cyanobacterial AP (Extended Data Fig. 6a). This migration was triggered only after an additional lag of 1–8 hours after sulfide depletion, depending on the O_2 and sulfide levels in the overlying water (Extended Data Fig. 6b). The ensuing exposure of cyanobacteria to a higher photon flux at the mat surface resulted in high rates of OP and AP and the onset of net O_2 export. As the vertical structure of the mat persisted during subsequent lower light intensities, rates of both OP and AP remained high (Fig. 3e).

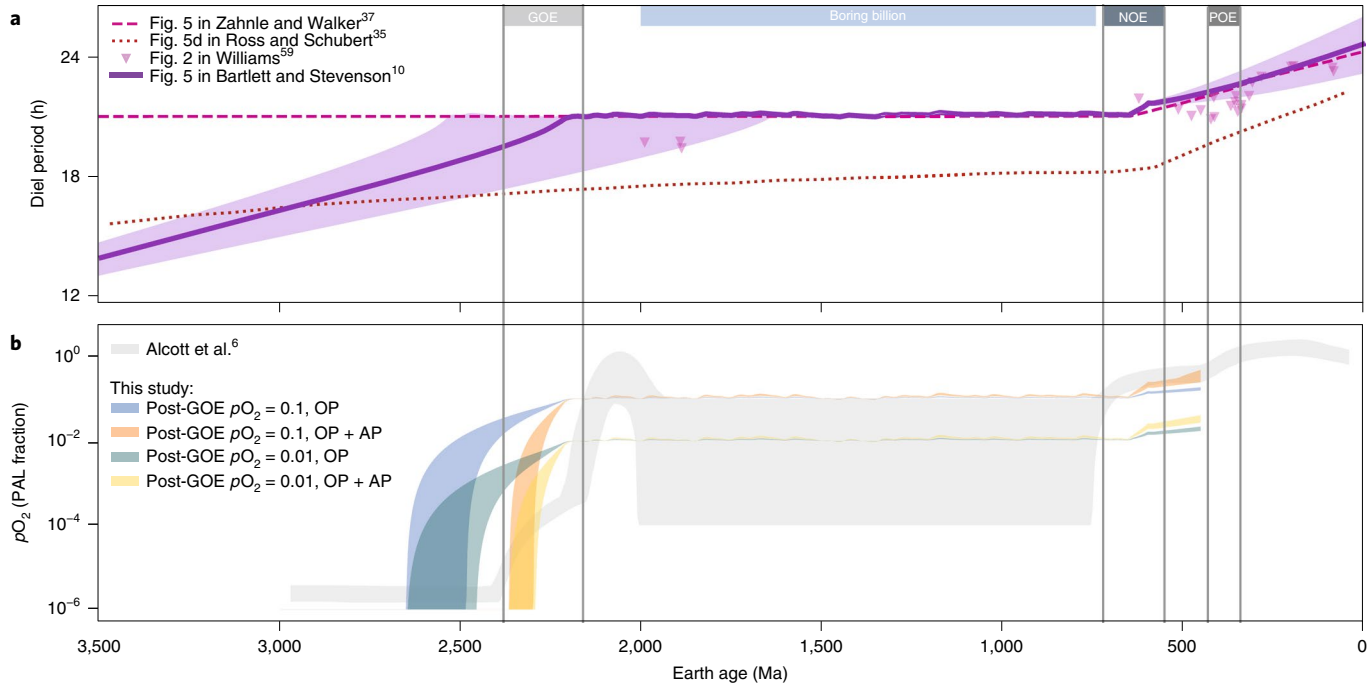

Fig. 4 | Interaction of Earth's daylength and oxygenation. a, Estimates for modelled and empirical values for daylength as derived from various studies[10,35,37,59], illustrate that daylength might have been nearly constant in the Proterozoic. This coincides with the boring billion[6], and the Earth escaped the 'resonance lock' in the timeframe of the NOE. **b**, Estimates of the quasi-steady states of the global reservoir of pO_2 as a response to changes in coastal benthic and terrestrial C_{org} burial fluxes driven by changes in daylength. The proposed daylength effect on microbial mat fluxes was calculated based on the Earth rotation model by Bartlett and Stevenson[10] (solid line in **a**). daylength can account for a substantial portion of the pO_2 changes associated with the GOE and NOE, which lead up to the POE. The oxygenation scheme (grey area) is shown for comparison and is adapted from Alcott et al.[6]. Fluxes are derived from our modelled scenarios, which represent systems that include R_{aero} and R_{anaero} and either exclusive oxygenic or partitioned OP and AP (scenarios 'OP SRB' and 'OP SRB + AP'). Scenarios with metabolic delay mechanisms or a steep dependency on the burial of O_2 were excluded because these yielded oscillations of pO_2 between 0 and 1 even in the boring billion years. Shaded areas represent the range of daylength-driven pO_2 change based on a 1.5–3.7% coverage of the modern oceanic area by benthic coastal mats (which corresponds to 20–50% of the global marine C_{org} burial during the mid-Proterozoic) and a coverage of 5% of the continental area by terrestrial mats. The corresponding global O_2 sinks were parameterized for a reference pO_2 of 0.1 and 0.01 in the mid-Proterozoic[60]. For terrestrial mats we assumed a direct interaction of 95% of their buried C_{org} with pO_2 by erosional weathering, which represents a negative feedback effect of daylength-driven C_{org} burial on pO_2.

The chemosynthetic SOB modulated the locally availability of light for cyanobacteria and caused delayed O_2 production, which implies a strong effect of daylength on the net O_2 export from mats that host competitive photosynthetic and chemosynthetic communities. We assessed this prediction by measuring the net O_2 production in these mats during different daylengths simulated in the laboratory under low O_2 conditions (Figs. 2a and 3f, and Extended Data Fig. 7). For daylengths of <12 hours, no O_2 was produced and the mats were a net sink for O_2. For a daylength of 16 hours (that is, late Archean) and longer, a net diel O_2 export occurred, with 21 hour (late Proterozoic) and 24 hour daylengths exporting two and three times, respectively, more O_2 than 16 hour one.

Although similar competitive effects have been observed in other extant mat systems[26], the applicability of these analogues to Precambrian mats is uncertain. However, several other mechanisms also result in a delayed O_2 production due to a dramatic variation of the redox conditions in microbial mats within diel timescales. Some microbial groups are equipped with mechanisms to regulate or delay the onset of certain metabolic processes[20,27–29]. Similar to the MIS mat, the implementation of a delayed recovery of OP after exposure to sulfide[27] in our modelled mat showed that GPP and C_{org} burial decreased sharply with decreasing daylength (Extended Data Fig. 8). Overall, the combined effect of mass transfer limitation, metabolic regulation and whole-community interactions in living microbial mats strengthens the dependency of O_2 export and C_{org} burial on increasing daylength (Fig. 2).

The regulation of C_{org} burial by daylength and by the corresponding diel O_2 dynamics is conceptually consistent with empirical observations in modern sediments, in which the long-term burial efficiency decreases with the exposure time to O_2 (ref. [14]). As longer days export more O_2, the ratio between R_{aero} and R_{anaero} decreases (Extended Data Fig. 3), the average diel O_2 penetration depth decreases (Extended Data Fig. 2b) and the non-photosynthetic layers of mats are exposed to O_2 for a shorter fraction of the day (Extended Data Fig. 2c). This suggests that daylength also promotes long-term C_{org} burial independent of the effect of daylength on the dynamic response of respiratory processes with specific metabolic traits. Additionally, mat accretion rates must be accounted for because they shape the residence time of C_{org} in the oxic zone. Modern mats reach stunning accretion rates[30] (for example, 0.5–5 mm yr^{-1}), similar to estimates from ancient microbialites[31] (0.5–15 mm yr^{-1}). Given that longer days decreased the diel local O_2 availability and enhanced the burial efficiency, the accretion rate would have increased, thereby possibly establishing a positive feedback effect on long-term burial. This is because both regulatory factors result in shorter exposure times of benthic C_{org} to O_2, but on different timescales. Thus, the daylength effect on net productivity and long-term burial could possibly be more pronounced for growing mats than for our modelled mats with a stagnant biomass.

Spinning down to oxygenation

The fundamental effect of changing planetary rotation rate on benthic export fluxes would have applied for most of Earth's photosynthetic history until the end of the 'matworld'[32]. Quantitative assessment requires parameterizing global benthic C_{org} burial along with Earth's rotation rate, which decreased over Earth's history as inferred from geological proxies[33,34] and models[10,35]. A precise reconstruction of the rotation rate is currently beyond reach owing to uncertainties in the strengths of tidal friction, which includes effects from oceanic[33,36], atmospheric[10,37] and solid Earth tides[35]. Although there is no consensus on the exact pattern, the rate of oceanic tidal dissipation normalized to the strength of the astronomical forcing must have been lower than modern rates for long stretches of Earth's history because the current rate implies an Earth–Moon collision at ~1.5 Ga, for which there is no evidence[36]. Recent models that consider the effect of changes in the continental configuration on tidal dissipation rates suggest that Earth's rotational deceleration was lowest in the mid-Proterozoic[33]. Another long-standing hypothesis even predicts a period with a stable rotation rate in the Proterozoic due to a resonant atmospheric thermal tide[10,37]. The dissipation of oceanic and solid Earth tides cause rotational deceleration that is counteracted by atmospheric thermal tides, which depend on daylength[37]. This hypothesized period of stability and the subsequent marked increase in daylength coincide with the boring billion years of O_2 stasis and the NOE, respectively. The remarkable correlation between the patterns of Earth's oxygenation and rotation rate (Fig. 4) invites a quantitative evaluation of the potential mechanistic link between daylength and oxygenation.

We extended our estimates of diel benthic C_{org} burial to global scales over Earth's history. Considerations of C_{org} fluxes on planetary and geological scales require several uncertain assumptions, and thus our estimates represent a possible range of the effect of rotation rate on pO_2. To quantitatively implement Earth's rotational deceleration, we used a recent model[10], which predicts deceleration before 2.2 Ga followed by resonant stability during the mid-Proterozoic until ~650 Ma, and subsequent return to deceleration towards the modern 24 h daylength. To model the quasi-steady-state evolution of global pO_2, we considered that daylength-driven changes in global C_{org} burial and solute export fluxes interacted with sinks of O_2 beyond the benthic domain, namely, atmospheric reduction by metamorphism- and volcanism-derived gases and erosional weathering (Extended Data Fig. 1). As the relative contributions of benthic and pelagic to total marine C_{org} burial are highly uncertain[38–42], we expressed the benthic term as a fraction of total marine burial, assumed to be at modern levels. Beyond the marine realm, we considered the possible effect of terrestrial mats in the Precambrian[43]. As we expect long-term burial rates to be substantially lower than the diel C_{org} burial[14], we implemented a weathering-based negative feedback effect between pO_2 and terrestrial diel, and implicitly on long-term, C_{org} burial (Extended Data Figs. 1 and 9). This analysis showed that daylength-driven changes in C_{org} burial could account for the offset between pre- and post-GOE O_2 levels without having to assume any changes in atmospheric reductant fluxes or GPP (Fig. 4b). Mat scenarios with no net C_{org} burial in the pre-GOE Archean (18 h daylength) support 50% of the global marine C_{org} burial in the mid-Proterozoic (21 h daylength), but only occupy 3.7% of the modern oceanic area (see Methods). For the modern continental arrangement, this mat coverage is comfortably less than the neritic zone (7.5%)[44], the primary habitat for benthic photosynthesis. The daylength effect implies an increase up to ~0.28 pO_2 at around 0.55 Ga (Fig. 4b), consistent with an early NOE and a later Palaeozoic oxidation event (POE), possibly connected to the Great Ordovician Biodiversity Event, at ~0.4 Ga (refs [2,45]).

We suggest that changes in daylength rebalance remineralization. Positive carbon isotope excursions associated with oxygenation events are interpreted as signals of increased C_{org} burial, caused by increasing GPP or decreasing remineralization efficiency[46–48]. How these parameters imprint on the isotope record in the case of microbial mats is uncertain due to mass transfer limitation of dissolved inorganic carbon supply and the resultant negligible isotope fractionation observed in modern mats[49–51]. Yet, the daylength-driven enhancement of O_2 export and C_{org} burial is consistent with proxies for weathering and total organic carbon contents in the record (Extended Data Fig. 9). Despite the predicted increase in weathering, we have not included the response of phosphorus fluxes to increasing pO_2. Increased weathering would have further boosted the global primary production[7,52]—but probably only transiently as a pulse, followed by a return to the previous quasi-steady state pO_2 (refs [3,6]) for a given daylength. Although nutrient supply and the corresponding GPP determine the absolute range of pO_2 levels, daylength effects on benthic burial could have shaped the overall oxygenation pattern before the POE (Fig. 4b).

Overall, we show that increasing daylength is a monotonic driver of net productivity pervasive across all ranges of metabolic parameters (Fig. 2). Relatively abrupt changes in daylength, as caused by escape or entry into resonance locking, could therefore be among the triggers for the global oxidation events. In this respect, our proposed mechanism is similar to that of other abrupt events that cause imbalances in the global pO_2 budget, such as plate tectonics (including supercontinent formation)[5,53–55] or new prospects for productivity in the oceans and on land[4,45,56]. As Earth's rotation rate, governed by planetary physics, does not share any assumptions with these geological or biological triggers, the daylength effect operates in parallel to these other Earth-bound mechanisms. Even if we assume a more gradual decrease in rotation rate, our study clearly suggests that net productivity would have increased. Previous studies show that gradual changes in sources and sinks of O_2 can cause relatively abrupt shifts in pO_2, such as those due to H_2 escape, insolation, continental phosphorus supply, continental growth or volcanic reductant input[6,23,47,57,58]. The exact magnitude of the daylength effect remains uncertain as it relies on several assumptions, particularly the relationship between diel and long-term burial efficiency and the detailed pattern of rotational deceleration. Further, we have not considered the effects of changes in the limiting factors of gross productivity, such as phosphorus, insolation or strength of O_2 sinks, other than daylength-related increases in terrestrial C_{org} weathering. Yet, the peculiarity of daylength-driven increases in benthic net productivity is that no such changes are required to produce substantial changes in pO_2. Thus, the dynamics of the Earth–Moon system possibly had major impacts on global O_2 levels during critical turning points of Earth's biogeochemical evolution towards a profusely oxic world.

Online content

Any methods, additional references, Nature Research reporting summaries, source data, extended data, supplementary information, acknowledgements, peer review information; details of author contributions and competing interests; and statements of data and code availability are available at https://doi.org/10.1038/s41561-021-00784-3.

Received: 12 November 2020; Accepted: 31 May 2021;
Published online: 2 August 2021

References

1. Lyons, T. W., Reinhard, C. T. & Planavsky, N. J. The rise of oxygen in Earth's early ocean and atmosphere. *Nature* **506**, 307–315 (2014).
2. Och, L. M. & Shields-Zhou, G. A. The Neoproterozoic oxygenation event: environmental perturbations and biogeochemical cycling. *Earth Sci. Rev.* **110**, 26–57 (2012).
3. Lenton, T. M., Boyle, R. A., Poulton, S. W., Shields-Zhou, G. A. & Butterfield, N. J. Co-evolution of eukaryotes and ocean oxygenation in the Neoproterozoic era. *Nat. Geosci.* **7**, 257–265 (2014).

4. Brocks, J. J. et al. The rise of algae in Cryogenian oceans and the emergence of animals. *Nature* **548**, 578–581 (2017).
5. Williams, J. J., Mills, B. J. & Lenton, T. M. A tectonically driven Ediacaran oxygenation event. *Nat. Commun.* **10**, 2690 (2019).
6. Alcott, L. J., Mills, B. J. W. & Poulton, S. W. Stepwise Earth oxygenation is an inherent property of global biogeochemical cycling. *Science* **366**, 1333–1337 (2019).
7. Reinhard, C. T. et al. Evolution of the global phosphorus cycle. *Nature* **541**, 386–389 (2017).
8. Lambeck, K. *The Earth's Variable Rotation: Geophysical Causes and Consequences* (Cambridge Univ. Press, 1980).
9. Munk, W. H. & MacDonald, G. J. F. *The Rotation of the Earth: A Geophysical Discussion* (Cambridge Univ. Press, 1960).
10. Bartlett, B. C. & Stevenson, D. J. Analysis of a Precambrian resonance-stabilized day length. *Geophys. Res. Lett.* **43**, 5716–5724 (2016).
11. Ćuk, M. & Stewart, S. T. Making the Moon from a fast-spinning Earth: a giant impact followed by resonant despinning. *Science* **338**, 1047–1052 (2012).
12. Chennu, A. MicroBenthos: a modeling framework for microbial benthic ecology. *J. Open Source Softw.* **3**, 674 (2018).
13. Lalonde, S. V. & Konhauser, K. O. Benthic perspective on Earth's oldest evidence for oxygenic photosynthesis. *Proc. Natl Acad. Sci. USA* **112**, 995–1000 (2015).
14. Sarmiento, J. L. & Gruber, N. in *Ocean Biogeochemical Dynamics* (eds Sarmiento, J. L. & Gruber, N.) 227–269 (Princeton Univ. Press, 2006).
15. Shen, Y. & Buick, R. The antiquity of microbial sulfate reduction. *Earth Sci. Rev.* **64**, 243–272 (2014).
16. Reinhard, C. T. et al. Proterozoic ocean redox and biogeochemical stasis. *Proc. Natl Acad. Sci. USA* **110**, 5357–5362 (2013).
17. Fründ, C. & Cohen, Y. Diurnal cycles of sulfate reduction under oxic conditions in cyanobacterial mats. *Appl. Environ. Microbiol.* **58**, 70–77 (1992).
18. Canfield, D. E. & Des Marais, D. J. Aerobic sulfate reduction in microbial mats. *Science* **251**, 1471–1473 (1991).
19. Canfield, D. E. & Des Marais, D. J. Biogeochemical cycles of carbon, sulfur, and free oxygen in a microbial mat. *Geochim. Cosmochim. Acta* **57**, 3971–3984 (1993).
20. Klatt, J. M. et al. Anoxygenic photosynthesis controls oxygenic photosynthesis in a cyanobacterium from a sulfidic spring. *Appl. Environ. Microbiol.* **81**, 2025–2031 (2015).
21. Sánchez-Baracaldo, P. Origin of marine planktonic cyanobacteria. *Sci. Rep.* **5**, 17418 (2015).
22. Valentine, J. W. & Moores, E. M. Plate-tectonic regulation of faunal diversity and sea level: a model. *Nature* **228**, 657–659 (1970).
23. Feulner, G. The faint young Sun problem. *Rev. Geophys.* **50**, RG2006 (2012).
24. Olson, S. L., Jansen, M. & Abbot, D. S. Oceanographic considerations for exoplanet life detection. *Astrophys. J.* **895**, 19 (2020).
25. Voorhies, A. A. et al. Cyanobacterial life at low O_2: community genomics and function reveal metabolic versatility and extremely low diversity in a Great Lakes sinkhole mat. *Geobiology* **10**, 250–267 (2012).
26. Klatt, J. M. et al. Structure and function of natural sulphide-oxidizing microbial mats under dynamic input of light and chemical energy. *ISME J.* **10**, 921–933 (2016).
27. Hamilton, T. L., Klatt, J. M., de Beer, D. & Macalady, J. L. Cyanobacterial photosynthesis under sulfidic conditions: insights from the isolate *Leptolyngbya* sp. strain hensonii. *ISME J.* **12**, 568–584 (2018).
28. Oren, A. & Padan, E. Induction of anaerobic, photoautotrophic growth in the cyanobacterium *Oscillatoria limnetica*. *J. Bacteriol.* **133**, 558–563 (1978).
29. Garcia-Pichel, F. & Castenholz, R. W. Comparative anoxygenic photosynthetic capacity in 7 strains of a thermophilic cyanobacterium. *Arch. Microbiol.* **153**, 344–351 (1990).
30. Krumbein, W. E., Cohen, Y. & Shilo, M. Solar Lake (Sinai). 4. Stromatolitic cyanobacterial mats. *Limnol. Oceanogr.* **22**, 635–656 (1977).
31. Lanier, W. P. Approximate growth rates of early Proterozoic microstromatolites as deduced by biomass productivity. *Palaios* **1**, 525–542 (1986).
32. Lenton, T. M. & Daines, S. J. Matworld—the biogeochemical effects of early life on land. *New Phytol.* **215**, 531–537 (2016).
33. Meyers, S. R. & Malinverno, A. Proterozoic Milankovitch cycles and the history of the solar system. *Proc. Natl Acad. Sci. USA* **115**, 6363–6368 (2018).
34. Williams, G. E. Late Precambrian tidal rhythmites in South Australia and the history of the Earth's rotation. *J. Geol. Soc.* **146**, 97–111 (1989).
35. Ross, M. N. & Schubert, G. Evolution of the lunar orbit with temperature- and frequency-dependent dissipation. *J. Geophys. Res.* **94**, 9533 (1989).
36. Bills, B. G. & Ray, R. D. Lunar orbital evolution: a synthesis of recent results. *Geophys. Res. Lett.* **26**, 3045–3048 (1999).
37. Zahnle, K. & Walker, J. C. A constant daylength during the Precambrian era? *Precambrian Res.* **37**, 95–105 (1987).
38. Gueneli, N. et al. 1.1-billion-year-old porphyrins establish a marine ecosystem dominated by bacterial primary producers. *Proc. Natl Acad. Sci. USA* **115**, E6978–E6986 (2018).
39. Sergeev, V. N., Gerasimenko, L. M. & Zavarzin, G. A. The Proterozoic history and present state of cyanobacteria. *Microbiology* **71**, 623–637 (2002).
40. Demoulin, C. F. et al. Cyanobacteria evolution: insight from the fossil record. *Free Radic. Biol. Med.* **140**, 206–223 (2019).
41. Dodd, M. S., Papineau, D., Pirajno, F., Wan, Y. & Karhu, J. A. Minimal biomass deposition in banded iron formations inferred from organic matter and clay relationships. *Nat. Commun.* **10**, 5022 (2019).
42. Butterfield, N. J. Macroevolutionary turnover through the Ediacaran transition: ecological and biogeochemical implications. *Geol. Soc. Spec. Publ.* **326**, 55–66 (2009).
43. Finke, N. et al. Mesophilic microorganisms build terrestrial mats analogous to Precambrian microbial jungles. *Nat. Commun.* **10**, 4323 (2019).
44. Cahoon, L. B. in *Oceanography and Marine Biology, An Annual Review* (eds Ansell, A. et al.) 47–86 (Aberdeen Univ. Press, 1999).
45. Krause, A. J. et al. Stepwise oxygenation of the Paleozoic atmosphere. *Nat. Commun.* **9**, 4081 (2018).
46. Derry, L. A., Kaufman, A. J. & Jacobsen, S. B. Sedimentary cycling and environmental change in the Late Proterozoic: evidence from stable and radiogenic isotopes. *Geochim. Cosmochim. Acta* **56**, 1317–1329 (1992).
47. Hayes, J. M. & Waldbauer, J. R. The carbon cycle and associated redox processes through time. *Philos. Trans. R. Soc. Lond. B.* **361**, 931–950 (2006).
48. Des Marais, D. J., Strauss, H., Summons, R. E. & Hayes, J. M. Carbon isotope evidence for the stepwise oxidation of the Proterozoic environment. *Nature* **359**, 605–609 (1992).
49. Wieland, A., Pape, T., Möbius, J., Klock, J. H. & Michaelis, W. Carbon pools and isotopic trends in a hypersaline cyanobacterial mat. *Geobiology* **6**, 171–186 (2008).
50. Schidlowski, M., Gorzawski, H. & Dor, I. Carbon isotope variations in a solar pond microbial mat: role of environmental gradients as steering variables. *Geochim. Cosmochim. Acta* **58**, 2289–2298 (1994).
51. Des Marais, D. J. & Canfield, D. E. in *Microbial Mats* (eds Stal, L. J. & Caumette, P.) 289–298 (Springer, 1994).
52. Canfield, D. E., Poulton, S. W. & Narbonne, G. M. Late-Neoproterozoic deep-ocean oxygenation and the rise of animal life. *Science* **315**, 92–95 (2007).
53. Kump, L. R. & Barley, M. E. Increased subaerial volcanism and the rise of atmospheric oxygen 2.5 billion years ago. *Nature* **448**, 1033–1036 (2007).
54. Lee, C.-T. A. et al. Two-step rise of atmospheric oxygen linked to the growth of continents. *Nat. Geosci.* **9**, 417–424 (2016).
55. Campbell, I. H. & Allen, C. M. Formation of supercontinents linked to increases in atmospheric oxygen. *Nat. Geosci.* **1**, 554–558 (2008).
56. Butterfield, N. J. Early evolution of the Eukaryota. *Palaeontology* **58**, 5–17 (2015).
57. Zahnle, K. & Catling, D. Waiting for O_2. *Spec. Pap. Geol. Soc. Am.* **504**, 37–48 (2014).
58. Mills, B., Lenton, T. M. & Watson, A. J. Proterozoic oxygen rise linked to shifting balance between seafloor and terrestrial weathering. *Proc. Natl Acad. Sci. USA* **111**, 9073–9078 (2014).
59. Williams, G. E. Geological constraints on the Precambrian history of Earth's rotation and the Moon's orbit. *Rev. Geophys.* **38**, 37–59 (2000).
60. Daines, S. J., Mills, B. J. W. & Lenton, T. M. Atmospheric oxygen regulation at low Proterozoic levels by incomplete oxidative weathering of sedimentary organic carbon. *Nat. Commun.* **8**, 14379 (2017).

Methods

Modelling microbenthic O_2 export. We explored how microbial processes and export fluxes of their metabolic substrates and products from ancient benthic photosynthetic ecosystems were influenced by daylength, environmental conditions and various regulatory mechanisms of photosynthetic production and respiration using an in silico microbenthic model. Model scenarios were constructed and simulated using MicroBenthos software[12]. MicroBenthos model definitions and parameters for the described scenarios are provided with this article. The software and usage instructions are available at https://microbenthos.readthedocs.io.

The modelling framework is an adaptation of de Wit et al.[61]. Briefly, benthic systems are constructed as a diffusive–reactive system in a 1D computational domain, with discrete cells used to represent the spatial distribution of the state and parameter variables. While the study by de Wit et al.[61] focused on biomass growth running over long simulation times, our interest was to study the dynamics of process rates and solute fluxes over diel timescales. Therefore, we set a fixed biomass for the microbial groups, added a water subdomain on top of the sediment as a diffusive boundary layer and ran simulations until a diel steady state was reached (5 days). Our model domain used 5 µm cells, with an 8 mm sedimentary subdomain and 1 mm diffusive boundary layer of water on top. O_2 and sulfide concentrations were the state variables that we solved for. Photosynthetically active radiation (PAR) was expressed as a percent of the maximum intensity at the diel zenith, and followed a cosinusoidal pattern similar to that of diel insolation dynamics.

R_{aero} and SOX were formulated to occur throughout the sediment. Microbial groups (cyanobacteria and SRB) were represented as biomass distributions in the sediment subdomain, and biomass-dependent metabolism kinetics were expressed as multiplications of the response functions of salient environmental and state variables. Coupled partial differential equations of the state variables (O_2 and H_2S) were composed from the reaction terms that accounted for sediment porosity and were solved with finite-volume numerical approximations[62].

Our in silico mat allowed us to explore how diffusive mass transfer shapes the interplay between illumination dynamics, gross production and consumption rates, and diel O_2 export. The effect of daylength was studied by varying the period of the illumination from 12 h to 24 h, the range of estimated daylengths over Earth's history after the earliest estimates for the origin of OP[63]. We report the calculated average diel net export and process rates in units of mmol m^{-2} h^{-1} because the hour is the largest temporal unit unaffected by changes in the Earth's rotation and thus allows for comparison across daylengths.

First, we explored the simplest case of O_2 production, which is with light availability. Two microbial processes were considered: OP performed by cyanobacteria and R_{aero}. The parameters for the biotic reactions were re-expressed as a biomass-specific maximal yield (Q_{max}). A fundamental assumption is that the photosynthesis rate is strictly correlated to the instantaneous photon flux:

$$\mathrm{OP} = Q_{max} \times \mathrm{biomass} \times \mathrm{sat}\left(\mathrm{PAR}, K_{PAR}\right), \quad (1)$$

where sat is a Michaelis–Menten function with $K_{PAR} = 15\%$ and the cyanobacterial biomass with a log-normal distribution with a peak value of 12 mg cm^{-3} at 0.5 mm depth (Supplementary Video 1). The only source of O_2 is OP, and the sinks are aerobic (sedimentary) respiration (R_{aero}). For the production and consumption rates of C_{org}, we assumed a stoichiometry of:

$$H_2O + CO_2 \rightarrow O_2 + CH_2O \quad (2)$$

with respect to O_2 cycling rates, where CH_2O refers to one C_{org} equivalent. Assuming that C_{org} is predominantly particulate, with negligible diffusional transport, diel C_{org} burial was thus calculated as:

$$C_{org}\ \mathrm{buried} = \int \mathrm{OP} - \int R_{aero}, \quad (3)$$

where $\int$OP and $\int R_{aero}$ are the diel depth-integrated rates of O_2 production and consumption and are equivalent to C_{org} production and consumption according to equation (2). Thus, diel burial can also be represented through the export flux of O_2 at the top and bottom interfaces of the sedimentary domain:

$$C_{org}\ \mathrm{buried} = O_2\ \mathrm{export} = \int \mathrm{OP} - \int R_{aero}, \quad (4)$$

which allowed us to assess the dynamic steady state of the diel model when the average diel depth-integrated rates equalled the export fluxes.

To calibrate the O_2 productivity for unitless PAR intensities, we determined the Q_{max} that caused a maximum O_2 export that corresponded to the median maximal flux from illuminated benthic photosynthetic systems[13]. A Q_{max} of 4.0022 mmol g^{-1} h^{-1} produced the target export flux of 5.76 mmol m^{-2} h^{-1} under a sedimentary respiration load of 0.1 mM h^{-1}. Note that by calibrating the productivity to the maximum diel illumination, the model represents a 'mean solar day' of a given Earth year[59]. This allowed us to disentangle the effect of daylength from geological-scale changes in the insolation intensity, such as in the 'faint young Sun' paradigm reviewed thoroughly by Feulner[23], or changes in the solar spectrum related to atmospheric composition[64].

Next, we explored the effect of R_{anaero} on the daylength dependency of the process rates and export fluxes. We used the example of sulfate reduction performed by SRB with a log-normal biomass distribution with a peak value of 2 mg cm^{-3} (Supplementary Video 1). The R_{anaero} rate was either defined as a constant rate process for the scenario 'OP SRB constant' as:

$$R_{anaero} = Q_{max} \times \mathrm{biomass} \quad (5)$$

or as an O_2- and H_2S-sensitive process as:

$$R_{anaero} = Q_{max} \times \mathrm{biomass} \times \mathrm{inhibition}\left([O_2],\ K_{max,O_2},\ K_{half,O_2}\right) \times \mathrm{inhibition}\left([H_2S],\ K_{max,H_2S},\ K_{half,H_2S}\right) \quad (6)$$

where inhibition is a function of the local H_2S and O_2 concentration (x) of the form:

$$\frac{K_{max} - x}{2 \times K_{max} - K_{half} - x} \quad (7)$$

when $x < K_{max}$ and 0 when $x \geq K_{max}$. Inhibition factors chosen for both scenarios with O_2- and H_2S-sensitive SRB ('OP SRB' and 'OP SRB inhibited') were 3 mM for K_{max,H_2S}, 0.5 mM for K_{half,H_2S} and 1 µM for K_{half,O_2}. K_{max,O_2} was 0.8 mM for the scenario with a moderate inhibition, 'OP SRB', and 0.3 mM for the scenario with a strong inhibition, 'OP SRB inhibited'.

SOX was formulated as:

$$\mathrm{SOX} = k \times O_2 \times H_2S, \quad (8)$$

where $k = 351$ l mol^{-1} h^{-1} (ref. [65]). For R_{anaero} we assumed the stoichiometry:

$$SO_4^{2-} + 2CH_2O \rightarrow H_2S + 2CO_2 + 2H_2O, \quad (9)$$

and therefore calculated diel burial as:

$$C_{org}\ \mathrm{buried} = \int \mathrm{OP} - \int R_{aero} - 2 \times \int R_{anaero}, \quad (10)$$

where $\int R_{anaero}$ is the depth-integrated rate of sulfide production by SRB. The export flux of O_2 is shaped by mat-intrinsic rates of R_{aero}, OP and SOX according to:

$$O_2\ \mathrm{export} = \int \mathrm{OP} - \int R_{aero} - \int \mathrm{SOX}, \quad (11)$$

where $\int$SOX is the depth-integrated rate of O_2 consumption by SOX. Assuming the complete oxidation of H_2S to sulfate, H_2S export can be formulated as:

$$H_2S\ \mathrm{export} = \int R_{anaero} - 0.5 \times \int \mathrm{SOX}. \quad (12)$$

According to equations (10)–(12), diel burial can thus be represented as:

$$C_{org}\ \mathrm{buried} = O_2\ \mathrm{export} - 2 \times H_2S\ \mathrm{export} \quad (13)$$

This illustrates that the control of diel burial is related to the export of O_2 and the reduced product of R_{anaero} (such as H_2S), as the former is an equivalent source and the latter an equivalent sink of C_{org} within the mat. This means that an increase in O_2 export would not result in an increase of burial if H_2S export increased proportionally in terms of C_{org} equivalents.

To calibrate the productivity for SRB scenarios, we determined values of Q_{max} for OP and SRB, which yielded the target maximum export flux of 5.76 mmol m^{-2} h^{-1} at 24 h under 250 µM O_2 boundary conditions and negligible burial fluxes at 18 h under anoxic boundary conditions, that is, in pre-GOE conditions (see Supplementary Data 1 for model parameters).

We tested the sensitivity of diel burial to O_2 concentration in the water column (0–250 µM) for all three SRB scenarios. For the least O_2-sensitive scenario ('OP SRB'), we also tested sensitivity of burial to gross productivity by varying the maximal photosynthetic yield Q_{max} over the range 0.5–10 mmol g^{-1} h^{-1}. Note that the variation in Q_{max} can be considered equivalent to variations in other factors that influence gross production, such as nutrient supply and irradiance levels.

We then explored the effect of AP and reductant supply to the mat. Reductants that served as electron donors for AP were available in Precambrian phototrophic habitats, and supported diverse forms of photosynthesis even after the GOE and the evolution of OP[66–68]. Although the extent and ecological niches of AP and OP over Earth's history remain unclear, AP and OP probably co-existed, with spatially and temporally variable partitioning of the total GPP between them[69]. Analogous to modern systems, the partitioning probably depended on the limiting factors of both metabolisms, such as light and nutrients, with AP additionally limited by electron donor supply, and on the onset of novel evolutionary avenues or geochemical transitions that facilitated shifts in the outcome of competition.

We implemented this concept by adapting the 'OP SRB' scenario to include metabolic flexibility in the modelled photosynthetic community, analogous to cyanobacteria that can partition harvested light energy towards OP and sulfide-driven AP (Extended Data Fig. 4). Transitions between photosynthetic modes are based on the local sulfide and light availability with the rate of OP regulated by the rate of AP[20]. In this 'OP SRB + AP' scenario, the modelled cyanobacteria produced O_2 according to:

$$\mathrm{OP} = Q_{\max} \times \mathrm{biomass} \times \mathrm{sat}(\mathrm{PAR}, K_{\mathrm{PAR}}) \times (1 - \mathrm{normsat}(\mathrm{H_2S}, \mathrm{H_2S_{thr}})), \quad (14)$$

where normsat is a normalized Michaelis–Menten function with a value of 1 for $H_2S \geq H_2S_{thr}$, where H_2S_{thr} is the threshold sulfide level. Conversely,

$$\mathrm{AP} = Q_{\max} \times \mathrm{biomass} \times \mathrm{sat}(\mathrm{PAR}, K_{\mathrm{PAR}}) \times \mathrm{normsat}(\mathrm{H_2S}, \mathrm{H_2S_{thr}}) \quad (15)$$

The metabolic behavior is such that OP occurs only below H_2S_{thr}, which is light dependent. Below this threshold level, the harvested light energy is partitioned towards AP and OP, with a higher affinity for AP. Above the threshold, only AP occurs and OP is suppressed. The resulting metabolic response is that the sum of OP and AP follows the form of equation (1), whereas R_{anaero}, R_{aero}, SOX and other processes work as in previous scenarios. The interplay of illumination, mat processes and the resultant depth-resolved dynamics of O_2 and H_2S under this scenario can be seen in the Supplementary Video 1. Assuming sulfate as the product of AP according to:

$$H_2S + 2CO_2 + H_2O \rightarrow SO_4^{2-} + 2CH_2O, \quad (16)$$

diel burial in this scenario was calculated as

$$C_{org}\ \mathrm{buried} = \int \mathrm{OP} + \int \mathrm{AP} - \int R_{aero} - 2 \times \int R_{anaero}, \quad (17)$$

where $\int$AP is the depth-integrated rate of CO_2 fixation by AP. As in the other scenarios, diel burial can alternatively be calculated according to equation (13). Values of Q_{max} for OP and R_{anaero} were adjusted to produce the same maximum O_2 export flux at 24 h (O_2 boundary at 250 µM) and diel C_{org} flux at 21 h (25 µM O_2 boundary) as in 'OP SRB'. This allowed us to establish directly comparable upscaling calculations for global pO_2 at the same areal coverage and diel burial by 'OP SRB' and 'OP SRB + AP' mats (see below).

Besides the effect of daylength, we also studied the effect of the availability of O_2 and H_2S as electron donors from the water column on the scenario with AP. Water column O_2 levels from 0 to 250 µM and H_2S levels from 0 to 20 µM were tested.

Photosynthetic inhibitory mechanisms were also tested by modelling cyanobacteria that exhibit a 30 min recovery time of OP after the local sulfide levels fall below a certain level[27].

Microsensor measurements. We sampled cores from cyanobacterial mats that formed in the MIS (Michigan, United States) in October 2015, May 2016 and June 2016. Cores and bottom water sampled from above the mats were transported to the lab in Ann Arbor. Cores were either used directly or kept on the seasonal day–night light cycle at 8 °C until the measurements were made. During the measurements in the cores, a circular flow of the water column above the mat surface was adjusted using peristaltic pumps connected to an external temperature-controlled reservoir of bottom water. Water column O_2 and sulfide concentrations were adjusted in this separate reservoir of bottom water using N_2, air and neutralized Na_2S solution. After adjustment, the reservoir was covered with paraffin oil to prevent gas exchange and maintain constant conditions in the water column. The total sulfide concentration in the water column was regularly checked by subsampling and colorimetric determination according to Cline[70]. Both the water column reservoir and the core were kept at 10 °C during the measurements.

Illumination was provided by a broadband halogen lamp (Schott KL-1500). In situ spectral light quality was simulated using optical filter foils (Roscolux 375, Rosco Laboratories). The incident irradiance at the surface of the mat was determined with a submerged cosine-corrected quantum sensor connected to a LI-250A light meter (both LI-COR Biosciences GmbH). O_2, pH and H_2S microsensors with a tip diameter of 10–50 µm and a response time of <1 s were built, calibrated and employed as previously described[71–73]. The microsensor tips were always separated by <500 µm during simultaneous O_2, pH and H_2S measurements.

The volumetric rates of gross OP were estimated based on the dynamics of O_2 concentration after a light–dark shift, as described previously[74]. Analogously, the volumetric rates of gross AP were calculated from the increase of H_2S concentration and pH directly after a light–dark transition (that is, light-driven S_{tot} consumption rates), as previously described[26,27,75]. Net rates and fluxes were calculated from profiles based on Fick's laws using diffusion coefficients for O_2 and sulfide corrected for temperature and salinity.

From diel export to global oxygenation. We considered that changes in diel O_2 and H_2S export rates, the difference of which is equivalent to diel benthic C_{org} burial, interact with global redox controls beyond the mat domain (Extended Data Fig. 1). Namely, we considered atmospheric reduction by volcanism- and metamorphism-derived gases (atmR) and weathering[60]. Although we assumed a constant flux of reductant (vR) available for atmospheric reduction, weathering is dependent on pO_2 and thus strongly tempers the accumulation of O_2 in the atmosphere. As a recent computational Earth rotation model[10] predicts a stabilized daylength in the mid-Proterozoic, we started our global calculations by assuming a pO_2 of 0.01–0.1 at the predicted stable 21 h. This pO_2 is the result of the interaction of global sources and sinks (illustrated in Extended Data Fig. 1) according to a simplified version of the formulations (for example, COPSE[60,76]) of the global O_2 budget. Considering an evolution of steady states of pO_2 throughout Earth's history, we described the pO_2 evolution at a given age as:

$$\frac{\mathrm{d}(pO_2)}{\mathrm{d}t} = \mathrm{pB} + \mathrm{mB} - \mathrm{vR} - (0.95 \times \mathrm{tB} + \mathrm{uB}) \times pO_2^{0.5}, \quad (18)$$

which provides the steady state pO_2 as:

$$pO_2 = \left(\frac{\mathrm{pB} + \mathrm{mB} - \mathrm{vR}}{0.95 \times \mathrm{tB} + \mathrm{uB}}\right)^2, \quad (19)$$

where pB is the global burial flux associated with marine pelagic production, mB is total mat burial flux, vR is the flux of volcanic reductant, tB is the burial flux by terrestrial mats, and uB is an aggregate flux term that captures uplift forcing, the global C_{org} reservoir and a weathering constant[60].

Changes in any of the global fluxes would therefore result in new steady state pO_2. For the total marine burial (pelagic pB and coastal benthic mB – tB) we assumed modern values throughout the Precambrian[60]. Beyond the marine realm, we considered the possible existence of terrestrial mats[43], which would have further boosted global GPP and C_{org} burial, but would have also been more susceptible to weathering (tB in Extended Data Fig. 1). For these terrestrial mats, we assumed the same regulation mechanisms of export fluxes as those for coastal benthic mats and considered that AP might have been driven by reductant supplied from R_{anaero}, but we did not explore the effects of external reductant availability for terrestrial mats. Using our diel mat model output for tB at 21 h daylength and for 5% continental coverage, we then calculated vR for the two pO_2 levels assuming the values for uB from Daines et al.[60].

The Earth rotation rate model[10] predicts monotonic deceleration before 2.2 Ga followed by a stable daylength of ~21 h due to the atmospheric thermal tide resonance until ~650 Ma, with a subsequent increase towards the modern 24 h daylength[10]. Starting at 21 h at 2 Gyr, we estimated the effect of the daylength-driven change in the C_{org} burial from benthic and terrestrial mats, the output of our diel mat model, on pO_2 levels both backwards and forwards in time. The modulation of pO_2 naturally depends on the steepness of the dependence of mat C_{org} burial on daylength (Fig. 2). However, we limited our analysis to the effect of mats with metabolic regulation from the moderately daylength-sensitive scenarios 'OP SRB' and 'OP SRB + AP'. Scenarios with a steeper dependency of burial on daylength yielded oscillations of pO_2 beyond PAL even due to the minimal variations in daylength within the resonant-locked phase in the mid-Proterozoic[10] and therefore had to be excluded from analysis of pO_2 evolution. We additionally included negative feedback effects of increasing pO_2 on the mat C_{org} burial by dynamically adjusting the O_2 boundary conditions in each time step according to the pO_2 calculated from the previous step. To then calculate the quasisteady-state pO_2 level based on changes in the benthic and terrestrial burial, the actual coverage and thus partitioning between the pelagic and benthic burial have to be considered. Reliable estimates for this partitioning are lacking. The presence of pelagic cyanobacteria has persisted since 1.1 Ga (ref. [38]). Yet, cyanobacteria in the palaeontological record are primarily benthic, with sparse evidence for pelagic forms[39–41]. Hypotheses for the limited pelagic productivity during the Proterozoic range from an inaccessible, toxic or damaging photic zone to late evolution of a planktonic lifestyle[21,66,77]. Alternatively, burial of the C_{org} produced by pelagic cyanobacteria might have been hindered by the small cell sizes, low sinking rates and resultant efficient remineralization within the water column[42,78]. The preservation of C_{org} by benthic microbial mats is as uncertain, especially when eroded—on land or in the oceans. In our calculations we considered the terrestrial erosional weathering explicitly (tB in Extended Data Fig. 1), which introduces a strong negative feedback effect on pO_2. This implicitly describes a substantial loss in translation of the diel C_{org} to long-term burial that we, however, did not explicitly account for. For marine benthic mats we argue that a more direct link between the diel and long-term burial of C_{org} is plausible given that mats can reach substantial thicknesses when undisturbed (for example, in Solar Lake the thickness is >1 m) (ref. [79]) and that mats have a similar remineralization fate as pelagic C_{org} export when eroded. To address these uncertainties, we considered benthic burial as between 20 and 50% of the total marine burial at 21 h daylength. Note that this partitioning must shift during our simulations over Earth history because benthic (and terrestrial) burial is daylength dependent, whereas we took an 'all is constant' approach for pelagic burial and the fraction of weathered diel C_{org}, as we expected a negligible effect of molecular diffusion and thus daylength on these fluxes.

Data availability

The datasets generated and analysed are available at https://doi.org/10.17617/3.66, and in the supplementary files with this paper. Source data are provided with this paper.

Code availability

The open source MicroBenthos framework (v0.15) was used to model the presented results. Documentation is available at https://microbenthos.readthedocs.io and the code at https://github.com/achennu/microbenthos.git. Model definition files specific to this study are included in the supplementary files. Software to simulate the daylength history was obtained from https://github.com/bencbartlett/lengthofday.

References

61. de Wit, R., Ende, F. P. & Gemerden, H. Mathematical simulation of the interactions among cyanobacteria, purple sulfur bacteria and chemotrophic sulfur bacteria in microbial mat communities. *FEMS Microbiol. Ecol.* **17**, 117–136 (1995).
62. Guyer, J. E., Wheeler, D. & Warren, J. A. FiPy: partial differential equations with Python. *Comput. Sci. Eng.* **11**, 6–15 (2009).
63. Fischer, W. W., Hemp, J. & Johnson, J. E. Evolution of oxygenic photosynthesis. *Annu. Rev. Earth Planet. Sci.* **44**, 647–683 (2016).
64. Arney, G. et al. The pale orange dot: the spectrum and habitability of hazy Archean Earth. *Astrobiology* **16**, 873–899 (2016).
65. Luther, G. W. et al. Thermodynamics and kinetics of sulfide oxidation by oxygen: A look at inorganically controlled reactions and biologically mediated processes in the environment. *Front. Microbiol.* **2**, 62 (2011).
66. Johnston, D. T., Wolfe-Simon, F., Pearson, A. & Knoll, A. H. Anoxygenic photosynthesis modulated Proterozoic oxygen and sustained Earth's middle age. *Proc. Natl Acad. Sci. USA* **106**, 16925–16929 (2009).
67. Jones, C., Nomosatryo, S., Crowe, S. A., Bjerrum, C. J. & Canfield, D. E. Iron oxides, divalent cations, silica, and the early earth phosphorus crisis. *Geology* **43**, 135–138 (2015).
68. Kharecha, P., Kasting, J. & Siefert, J. A coupled atmosphere–ecosystem model of the early Archean Earth. *Geobiology* **3**, 53–76 (2005).
69. Ozaki, K., Thompson, K. J., Simister, R. L., Crowe, S. A. & Reinhard, C. T. Anoxygenic photosynthesis and the delayed oxygenation of Earth's atmosphere. *Nat. Commun.* **10**, 3026 (2019).
70. Cline, J. D. Oxygenation of hydrogen sulfide in seawater at constant salinity, temperature and pH. *Environ. Sci. Technol.* **3**, 838–843 (1969).
71. Revsbech, N. P. An oxygen microsensor with a guard cathode. *Limnol. Oceanogr.* **34**, 474–478 (1989).
72. Jeroschewski, P., Steuckart, C. & Kühl, M. An amperometric microsensor for the determination of H_2S in aquatic environments. *Anal. Chem.* **68**, 4351–4357 (1996).
73. de Beer, D., Schramm, A., Santegoeds, C. M. & Kühl, M. A nitrite microsensor for profiling environmental biofilms. *Appl. Environ. Microbiol.* **63**, 973–977 (1997).
74. Revsbech, N. P. & Jørgensen, B. B. Photosynthesis of benthic microflora measured with high spatial resolution by the oxygen microprofile method: capabilities and limitations of the method. *Limnol. Oceanogr.* **28**, 749–759 (1983).
75. Klatt, J. M., de Beer, D., Häusler, S. & Polerecky, L. Cyanobacteria in sulfidic spring microbial mats can perform oxygenic and anoxygenic photosynthesis simultaneously during an entire diurnal period. *Front. Microbiol.* **7**, 1973 (2016).
76. Bergman, N. M., Lenton, T. M. & Watson, A. J. COPSE: a new model of biogeochemical cycling over Phanerozoic time. *Am. J. Sci.* **304**, 397–437 (2004).
77. Cockell, C. S. Ultraviolet radiation and the photobiology of Earth's early oceans. *Orig. Life Evol. Biosph.* **30**, 467–500 (2000).
78. Knoll, A. H., Summons, R. E., Waldbauer, J. R. & Zumberge, J. E. in *Evolution of Primary Producers in the Sea* (eds Falkowski, P. & Knoll, A.) 133–163 (Elsevier, 2007).
79. Krumbein, W. E. & Cohen, Y. Biogene, klastische und evaporitische Sedimentation in einem mesothermen monomiktischen ufernahen See (Golf von Aqaba). *Geol. Rundsch.* **63**, 1035–1065 (1974).
80. Lasaga, A. C. & Ohmoto, H. The oxygen geochemical cycle: dynamics and stability. *Geochim. Cosmochim. Acta* **66**, 361–381 (2002).
81. Nelson, D. C. & Castenholz, R. W. Light responses of *Beggiatoa*. *Arch. Microbiol.* **131**, 146–155 (1982).
82. Biddanda, B. A., McMillan, A. C., Long, S. A., Snider, M. J. & Weinke, A. D. Seeking sunlight: rapid phototactic motility of filamentous mat-forming cyanobacteria optimize photosynthesis and enhance carbon burial in Lake Huron's submerged sinkholes. *Front. Microbiol.* **6**, 930 (2015).
83. Klatt, J. M. et al. Versatile cyanobacteria control the timing and extent of sulfide production in a Proterozoic analog microbial mat. *ISME J.* **14**, 3024–3037 (2020).

Acknowledgements

We thank the technicians of the Microsensor Group for the sensor construction, V. Meyer (MPIMM) for advice during the measurements, D. de Beer (MPIMM), G. Druschel (IUPIU), H. Marchant (MPIMM), S. Grim (UofM) and S. Ruberg (NOAA GLERL) for discussions, and M. Medina, H. C. Tan, K. Olsen, O. Metcalf, K. Meyer, M. Powers and D. Smith from University of Michigan for their lab and logistical help. We are grateful for the support of R. Green, J. Bright, P. Hartmeyer, W. Lusardi, S. Gandulla and T. Smith from NOAA TBNMS. We thank B. C. Bartlett for making the Earth rotation simulation code available. This study was funded by NSF grants EAR1637066 and EAR1637093, NASA grant 80NSSC20K1135, the Max Planck Society and the University of Michigan Turner Fellowship.

Author contributions

J.M.K., B.K.A. and G.J.D. conceptualized the work. The methodology was provided by J.M.K. and A.C., the software by A.C., validation by J.M.K. and A.C., formal analysis by J.M.K. and A.C., investigation by J.M.K., resources by G.J.D., data curation by J.M.K. and A.C., original draft manuscript preparation by J.M.K., A.C. and G.J.D., draft review and editing by J.M.K., A.C., B.K.A., B.A.B. and G.J.D., visualization by J.M.K. and A.C., supervision by G.J.D. and funding acquisition by J.M.K., B.A.B. and G.J.D.

Competing interests

The authors declare no competing interests.

Additional information

Extended data is available for this paper at https://doi.org/10.1038/s41561-021-00784-3.

Supplementary information The online version contains supplementary material available at https://doi.org/10.1038/s41561-021-00784-3.

Correspondence and requests for materials should be addressed to J.M.K. or G.J.D.

Peer review information *Nature Geoscience* thanks Lee Kump, Timothy Lyons and the other, anonymous, reviewer(s) for their contribution to the peer review of this work. Primary Handling Editor: Rebecca Neely.

Reprints and permissions information is available at www.nature.com/reprints.

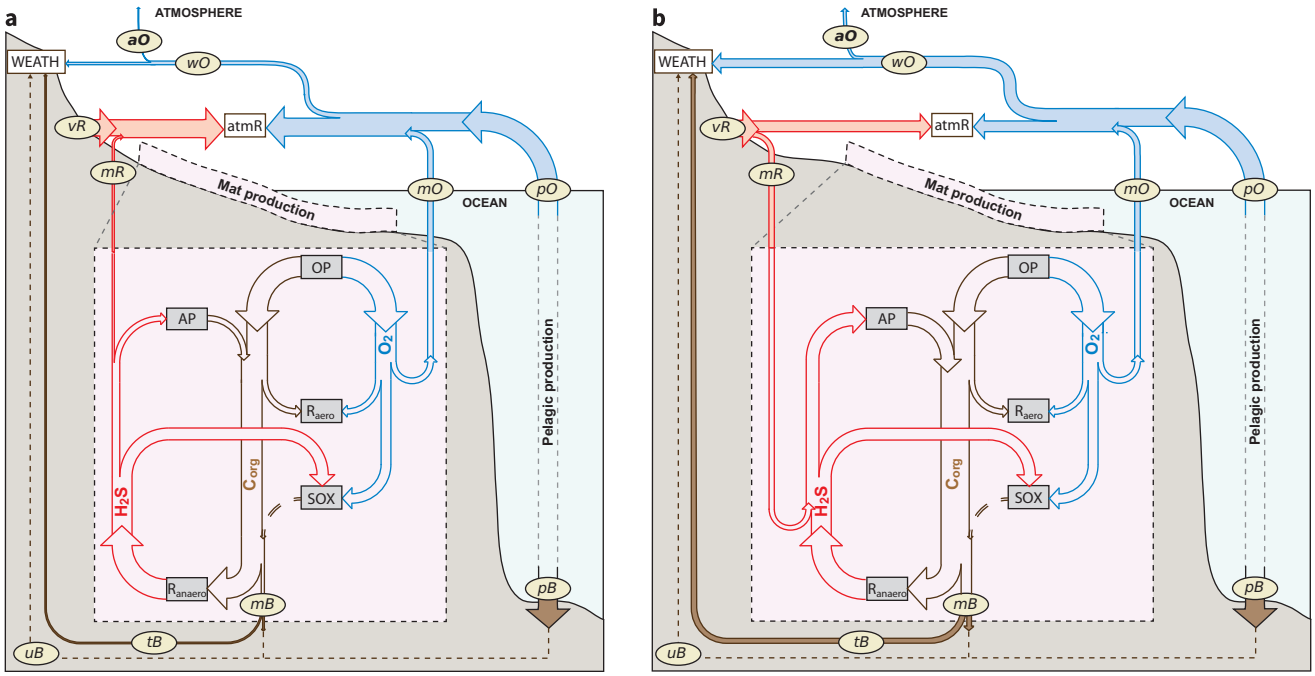

Extended Data Fig. 1 | Schematic of the global sinks and sources of O_2 with net release vs uptake of reductant by mats. The daylength-driven changes in C_{org} burial from benthic or terrestrial mats (mB; flux arrows not to scale) cause quasi steady-state transitions of global atmospheric pO_2. Offsets in pO_2 between such steady states are conceptualized here as aO. The diel mat processes (inset box) produce C_{org} burial fluxes (mB), which along with burial from the pelagic domain (pB) comprise the global O_2 source. Both O_2 (mO) and reductant (mR) export from mats are controlled by the interaction between mass transfer and mat-intrinsic process rates (oxygenic photosynthesis, OP; anoxygenic photosynthesis, AP; aerobic respiration, R_{aero}; sulfate reduction, R_{anaero}; aerobic H_2S oxidation, SOX), and hence are sensitive to daylength changes. For the global O_2 sinks, we considered that some of the surplus O_2 released from the terrestrial or marine realm was consumed directly in the atmosphere (atmR) by volcanism- and metamorphism-derived gases (vR)[60]. Surplus reductant released from mats (mR in (**a**)) will increase atmR. Surplus reductant consumed by mats (mR in (**b**)) will decrease atmR, and add to source strength mB. Thus, mat C_{org} burial mB is the sum of O_2 export mO and reductant import mR, and also sensitive to daylength. Note that volcanic reductant fluxes (vR) are equal to pelagic C_{org} burial (pB) and the equivalent pelagic O_2 export (pO) to illustrate that reductant uptake by mats influence the global availability of reductant. This influences the consumed fraction of pO by atmR. As a result, mB is equal to wO, *that is* the O_2 that escapes reduction by atmR. The sink for wO is erosional weathering (WEATH), and the emergent pO_2 for a reference weathering level is $(wO/(0.95 \times tB + uB))^2$ [76,80]. uB, which implicitly describes the size of the global C_{org} reservoir, uplift forcing and a weathering constant, was chosen based on a mid-Proterozoic pO_2 of 0.01 or 0.1 and was set constant over Earth age. To account for the direct erosion of terrestrial mats, WEATH was set to interact with 95% of terrestrial C_{org} burial rates (tB; a fraction of total mat burial mB). While this makes WEATH also sensitive to daylength and produces a buffering effect through increased weathering strength, atmospheric oxygenation aO still increases with daylength (Fig. 4).

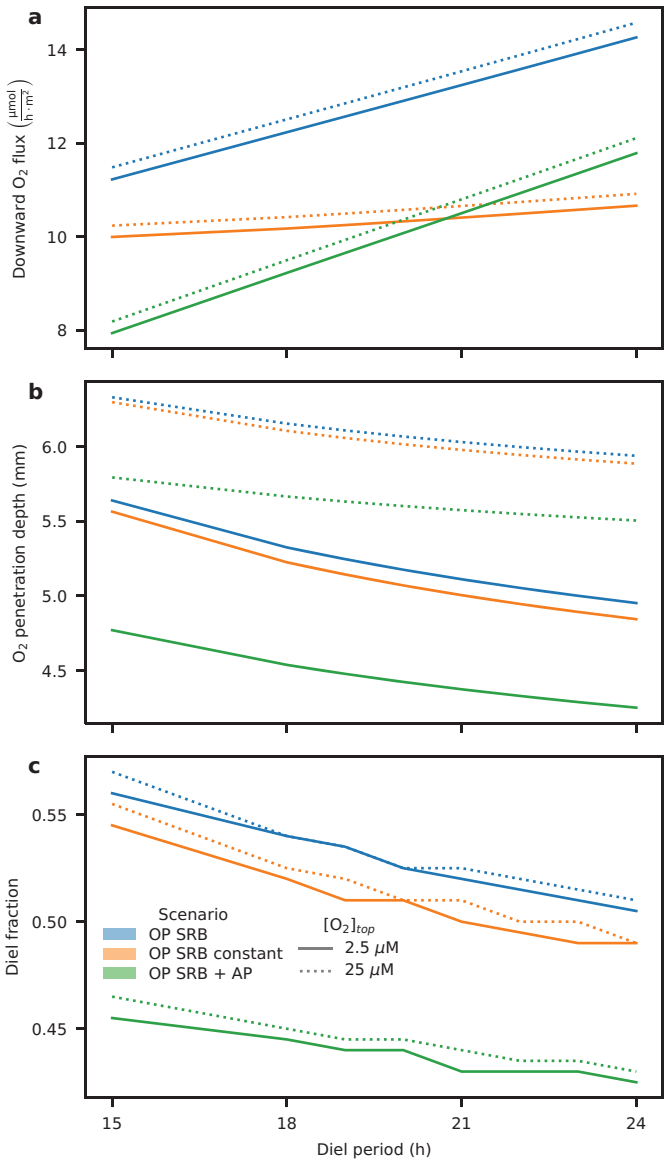

Extended Data Fig. 2 | Daylength-dependency of oxygen penetration depth, downward O_2 flux, and diel fraction with oxic conditions below the photic zone in various benthic mat scenarios. The total mat depth is 8 mm. **a**, Similar to the O_2 export flux across the upper mat interface, the downward flux is modulated by daylength. Given the proximity of the mat to the bottom substrate, such as pyrite, which is prone to abiotic oxidation reactions, this downward O_2 flux would increase pyrite weathering and sulfate release[13]. **b**, Despite the increase in fluxes, the diel oxygen penetration depth, measured as the depth which is exposed to at least 1µM O_2, decreases with daylength. **c**, Similarly, the fraction of a day, during which deep zones of the mat (here 7 mm) are exposed to > 1µM O_2 decreases with increasing daylength. Together, the factors in **b** & **c** represent a decrease of exposure time of deep C_{org} to O_2, and are likely to have boosted burial efficiency with increasing daylength.

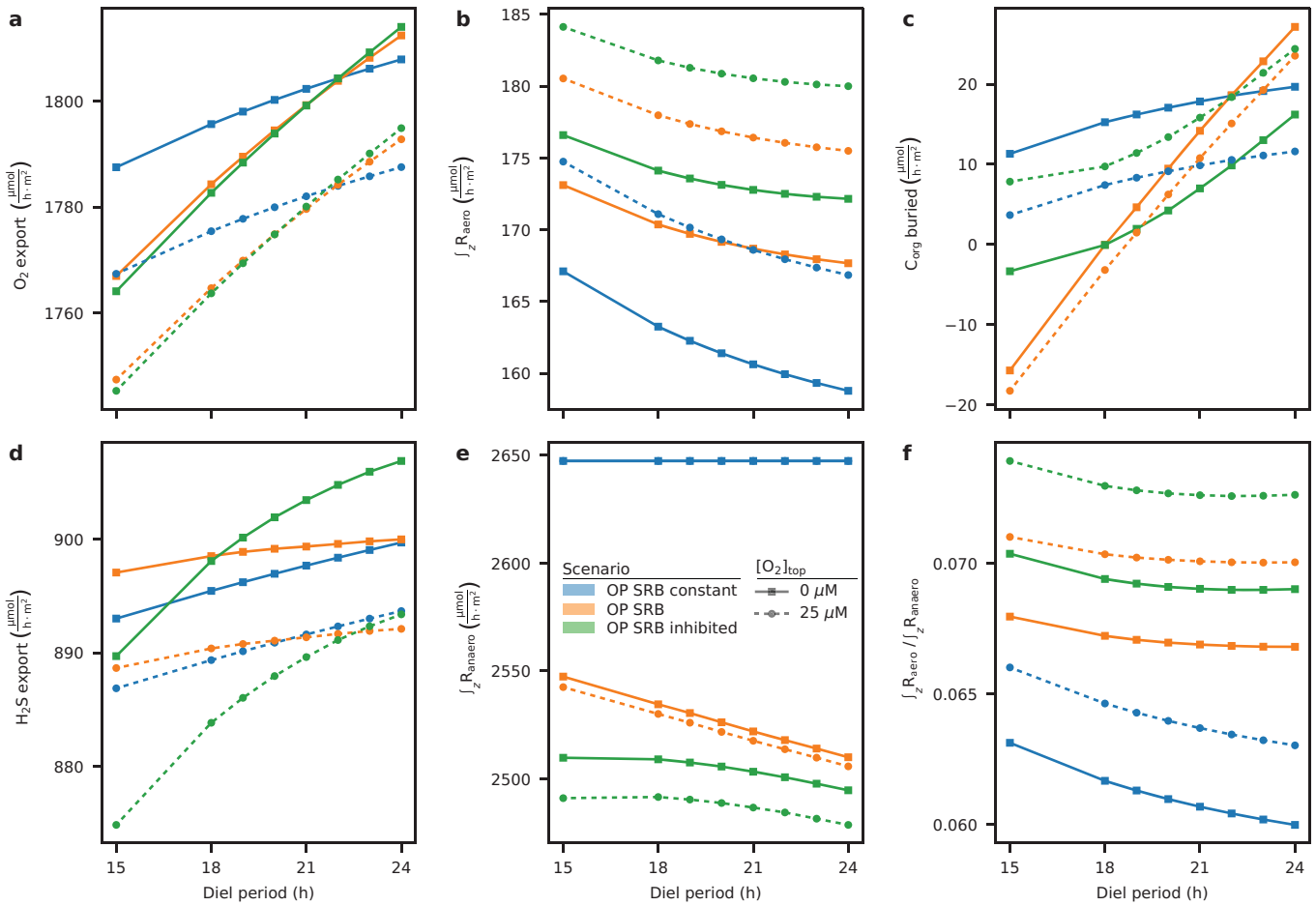

Extended Data Fig. 3 | Daylength-dependency of mat processes and export fluxes explored for three scenarios with differently adapted sulfate reducers. One scenario included anaerobic respiration that is not affected by changes in the O_2 concentrations within the mat (OP SRB constant), ie. with constant anaerobic respiration across daylengths. The other two scenarios (OP SRB and OP SRB inhibited) implement, with variable inhibition degree, O_2- and H_2S-sensitivity of anaerobic respiration rates[17–19]. As increasing O_2 in the water column ($[O_2]_{top}$) would have accompanied daylength increases over Earth's history, we explored daylength-dependent activity rates and export fluxes for O_2 boundary conditions 0 µM and 25 µM ($pO_2 = 0$ and 0.1 PAL). **a**, O_2 export consistently increases with daylength. **b**, Consequently, R_{aero} decreases. In the scenario with R_{anaero} set constant, R_{aero} is strongly enhanced under higher O_2 level in the water column. **c**, C_{org} burial, which is shaped by GPP, R_{aero}, R_{anaero} and diffusional mass transfer also increases with daylength. The increase of $[O_2]_{top}$ reduces burial for the scenario with constant R_{anaero} due to the increase in R_{aero}. Negative burial fluxes arise because model parameters were tuned such that burial approaches zero at 18 h (pre-GOE) for $[O_2]_{top}$ of 0 µM. **d**, H_2S export consistently increases with daylength. This implies that H_2S export partially counteracts the effect of increased O_2 export on burial compared to a purely aerobic scenario (Fig. 1)**. e**, For O_2-inhibited SRB, increasing water column O_2 reduces anaerobic respiration rates. Consequently, C_{org} burial consistently increases with daylength but remains approximately independent of $[O_2]_{top}$ in the scenario with moderate inhibition (OP SRB) and increases with $[O_2]_{top}$ in the scenario with strong inhibition (OP SRB inhibited) **f**, The ratio between respiratory processes R_{aero} and R_{anaero} decreases across scenarios and boundary conditions, indicating a rebalancing of remineralization activity due to daylength change. Empirical long-term C_{org} burial rates are negatively correlated with this ratio and the exposure time of C_{org} to O_2[14] (see Extended data figure 2).

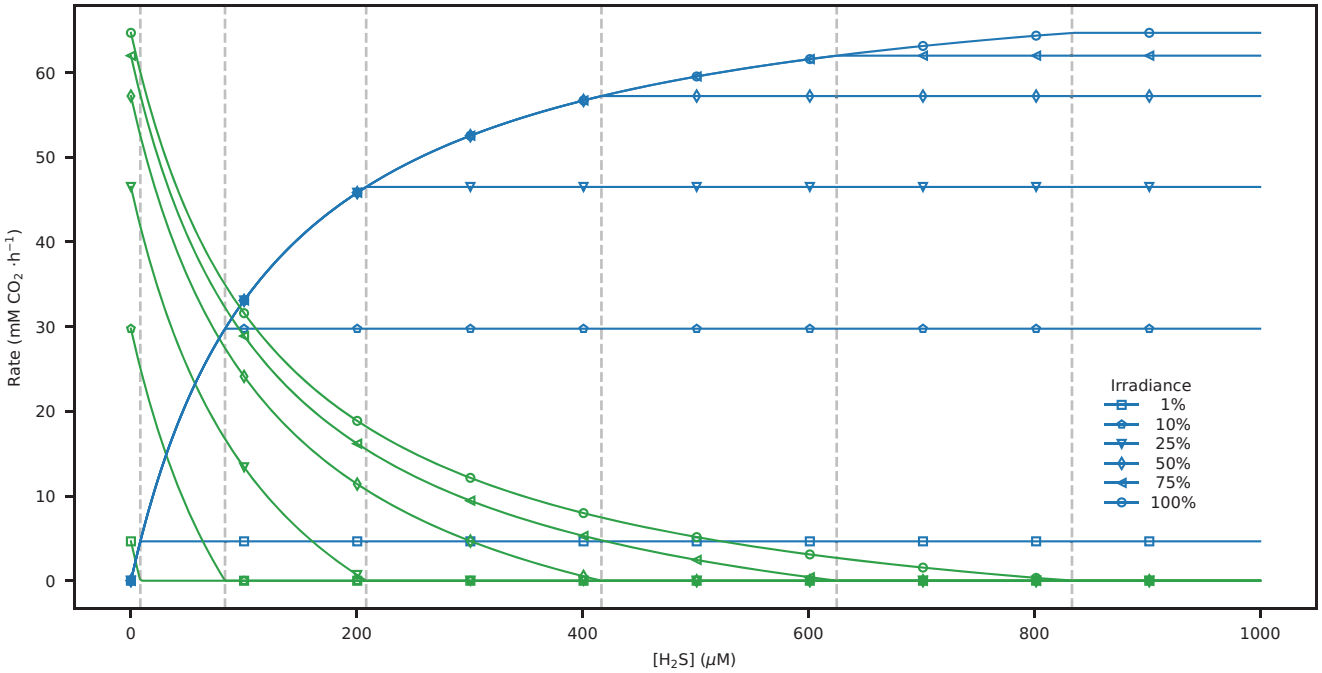

Extended Data Fig. 4 | Rates of cyanobacterial OP and AP depend on sulfide concentration and irradiance. (Irradiance as percent of zenith value) For conversion of CO_2 fixation rates into rates of photosynthetic O_2 production and sulfide consumption, we assumed that OP follows 2 H_2O + CO_2 → O_2 + C_{org} and AP follows H_2S + 2 CO_2 → SO_4^{2-} + 2 C_{org}, respectively. Partitioning between OP (green lines) and AP (blue lines) in these cyanobacteria is regulated through light-dependent sulfide threshold levels[20]. Below the threshold level, OP and AP occur in concert such that their combined rate (OP + AP) is conserved. Above the threshold level, only AP occurs representing a higher affinity for AP. This type of partitioning represents a metabolic competition between OP and AP within the cyanobacteria. Notably, based on local light levels, AP would have to occur at a sufficiently high rate to deplete the local sulfide concentration below the threshold for OP to occur and produce O_2.

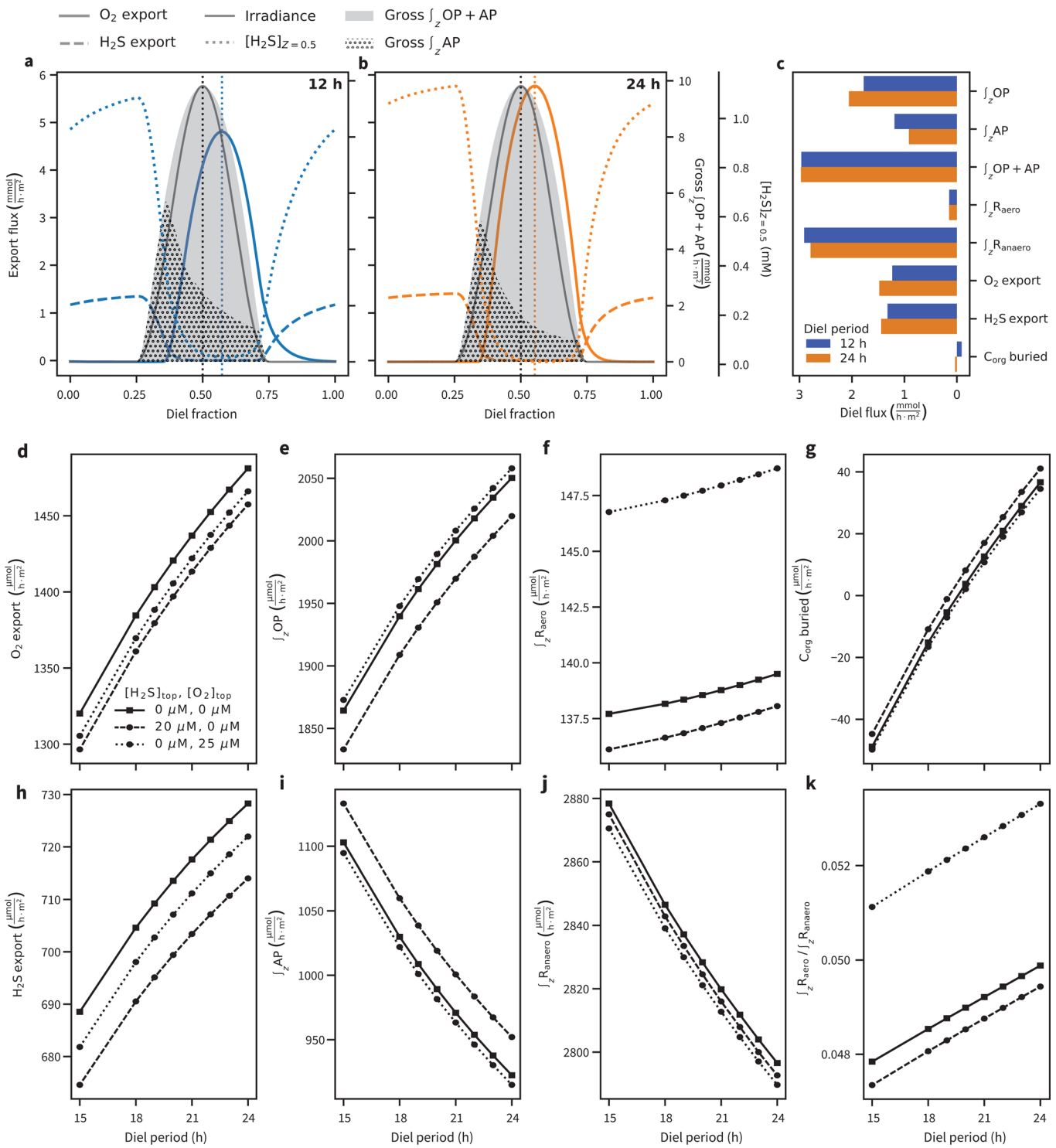

Extended Data Fig. 5 | Modeled temporal evolution of mat processes and export fluxes over 12 vs 24 h daylengths and and daylength-dependency of their diel averages explored for mat with AP. a & **b**, Based on partitioning regulation between AP (dotted fill) and OP (Extended data figure 4), AP first has to consume local sulfide (dotted line), after which OP occurs at its maximum light-dependent rate. Total photosynthesis ($\int_z P_{AP+OP}$, grey fill) remains independent of daylength. **c**, The overall effect of daylength is that longer days export more O_2 and bury more C_{org}. Note that the negative burial flux at 12 h arises because model parameters were tuned such that burial at 21 h is comparable to the scenario without AP (OP SRB in Extended data figure 3). **d-k**, As both reductant and O_2 exposure of the mat have varied temporally and spatially, we explored the sensitivity of daylength-dependent changes in mat processes and fluxes across various $[H_2S]_{top}$ and $[O_2]_{top}$ boundary conditions. Burial increases with increasing $[H_2S]_{top}$ and decreases with $[O_2]_{top}$. Yet, the effect of water column redox is negligible compared to the effect of daylength.

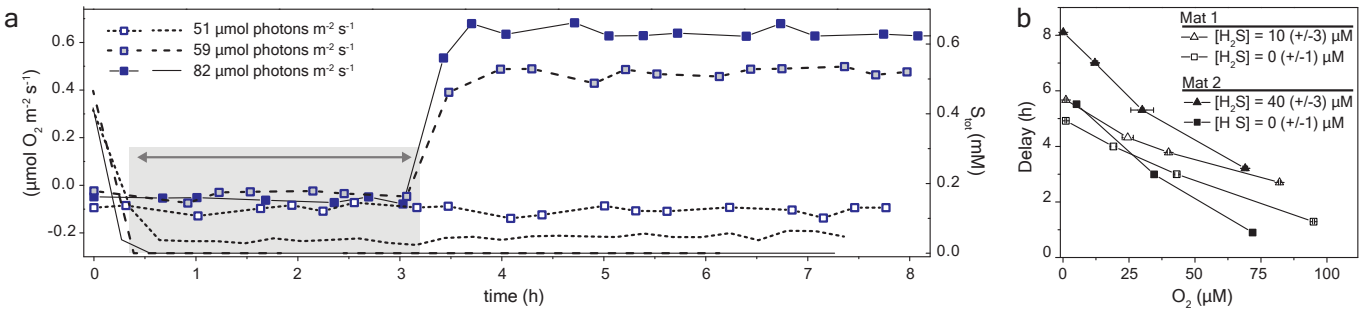

Extended Data Fig. 6 | Dependency of the lag duration of SOB migration in MIS mats on irradiance and water column concentrations of O_2 and H_2S. **a**, Net OP was calculated based on O_2 microsensor depth profiling at three light intensities in one MIS mat sample. Mat-forming large sulfur oxidizing bacteria (SOB) are known to respond to light and migrate downwards upon sunrise[81], while cyanobacteria are expected to migrate upwards[82]. However, similar to observations in the Frasassi Sulfidic Springs[26,83], MIS-SOB shade cyanobacteria and inhibit OP and showed no direct photophobic response. Instead, simultaneous depth profiling with an H_2S microsensor showed that migration only occurred if sulfide in the SOB layer was entirely depleted, such as after a sufficient duration of AP activity. Incident irradiance levels of 59 and 82 µmol photons m^{-2} s^{-1} were sufficiently high to allow for entire depletion of sulfide (solid and dashed lines in a) by AP in the cyanobacterial layer and to thereby limit sulfide supply to the SOB layer at the mat surface. The migration lag (~2.5 hours) after depletion of sulfide is indicated by the gray shaded area. Note that the duration of the lag is independent of light intensity. Light intensity of 51 µmol photons m^{-2} s^{-1} was insufficient for sulfide depletion (dotted lines) and consequently migration did not occurr. Thus, even though light had no direct effect on migration behavior, sufficient light intensity to sustain high rates of AP was necessary to deplete sulfide in order to trigger migration. **b**, The duration of the lag phase was monitored using an O_2 and H_2S microsensor under diverse water column conditions in two distinct mat samples. Irradiance during measurements was 73 and 103 µmol photons m^{-2} s^{-1} in mat 1 and mat 2, respectively. Data result from continuous profiling and involve an uncertainty of ~15-20 min due to the acquisition time of the profiles. Error bars and values in parenthesis in the legend represent the standard deviation of O_2 and H_2S concentration, respectively, averaged over three depths and 5-32 timepoints during the time series experiment (n=15-96 dependent on delay duration). Considering that increased sulfide supply from the water column extended the migration lag, migration might be induced via electron donor starvation of the SOB.

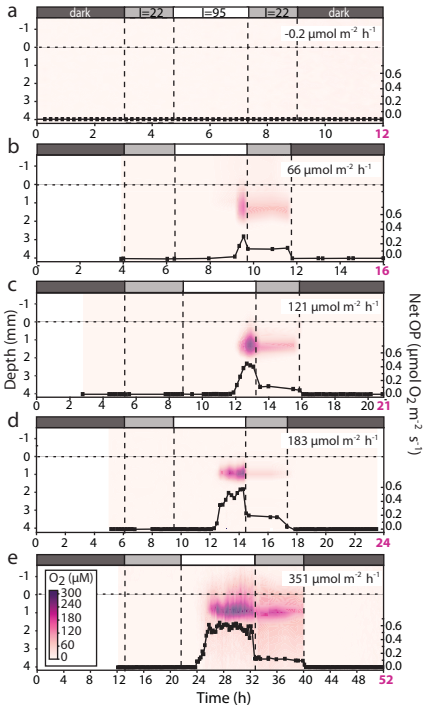

Extended Data Fig. 7 | Microsensor depth profiles of O_2 over simulated daylengths (12–52 h). a-e, Dynamics of O_2 export flux (solid lines) were calculated from the concentration depth profiles (color-coded maps) and used to estimate the diel period average (text in panel). Compiled export fluxes are shown in Fig. 3f. Light intensity during measurements is indicated by the top bar in µmol photons m^2 s^{-1}. Total sulfide concentration in the water column was <1 µM. Results highlight the substantial dependency of O_2 export on daylength in MIS mats.

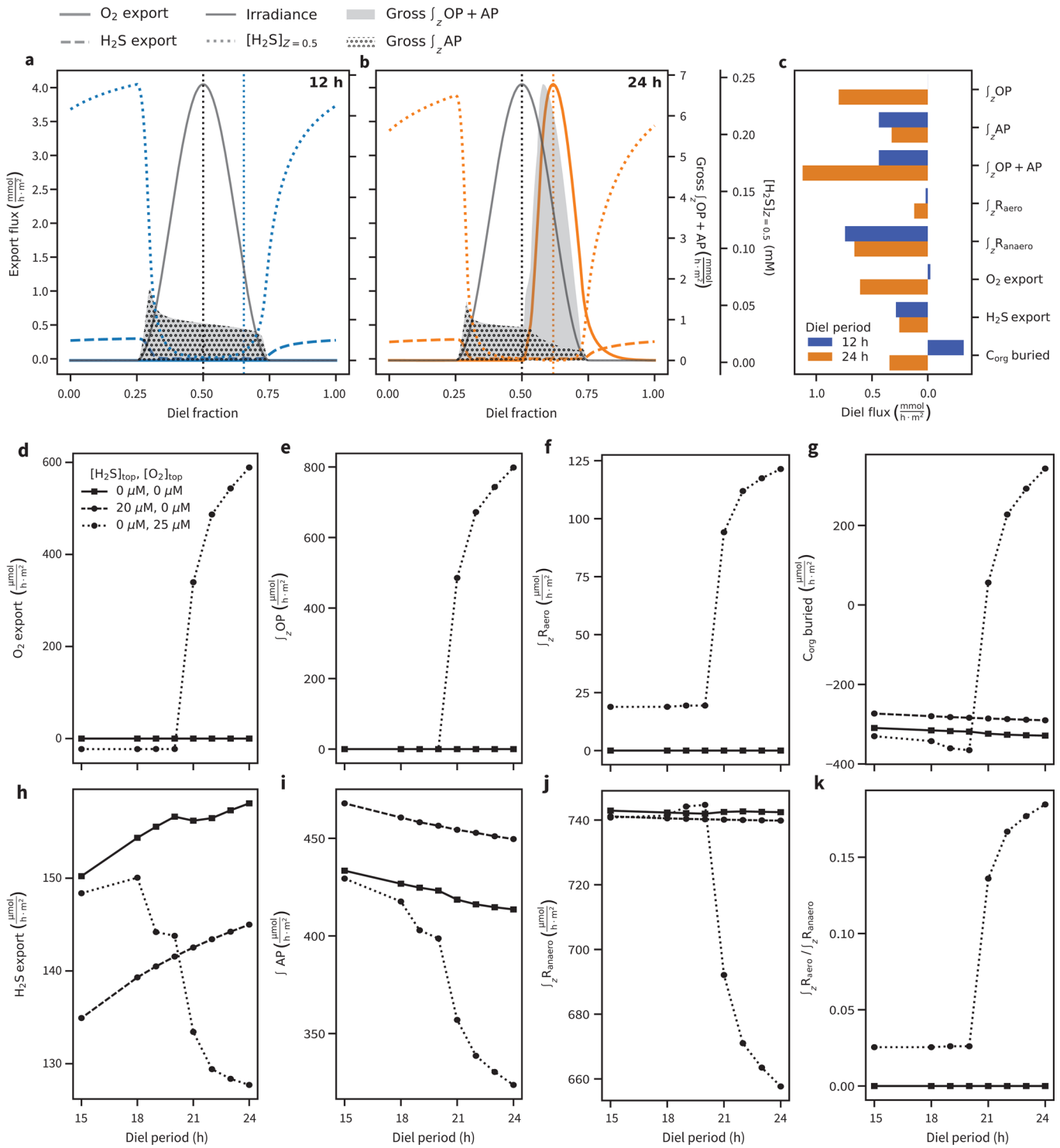

Extended Data Fig. 8 | Simulations of benthic systems with activity delay mechanisms. a-b, For sulfide-inhibited OP as observed in cyanobacteria isolated from Little Salt Spring, that only activate OP with a fixed delay of 30 min after local depletion of sulfide by AP[27], the temporal evolution over a 12 h and 24 h diel period illustrates that this no-photosynthesis-phase between sulfide being depleted below 1 μM and OP being activated completely suppresses OP in days shorter than 20 h (panel e). The penalty on O_2 export is high enough that cyanobacterial mats, despite the potential for OP, remain net sinks of O_2 during illuminated periods. **c**, The delay introduces a steep dependency of diel export fluxes and burial on daylength. Note that negative burial fluxes arise because model parameters were tuned such that burial at 21 h is comparable to the scenario without AP (OP SRB in Extended data figure 2) and the AP scenario without delay (Extended data figure 5). **d-k**, The penalty of the lag on induction of OP is only overcome during longer days and in the presence of O_2 in the water column ($[O_2]_{top}$). Mats can only net accumulate C_{org}, if OP is active. As the fraction of day during which OP can occur is strongly dependent on daylength, this scenario exhibits the steepest dependency of burial on daylength compared to all other scenarios.

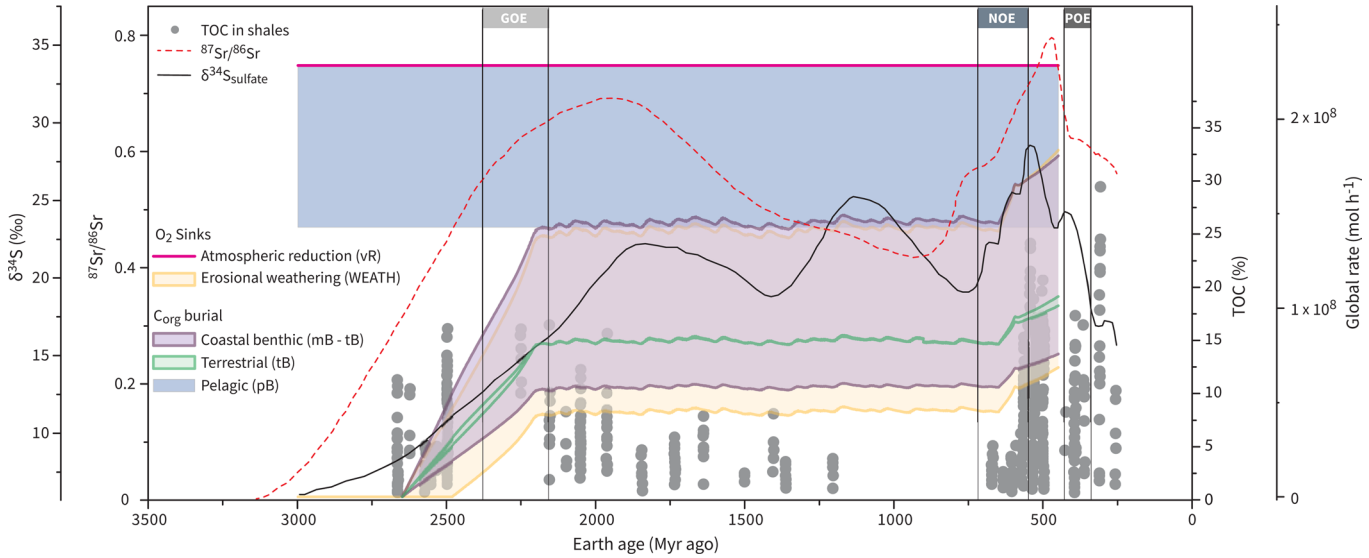

Extended Data Fig. 9 | Weathering and C_{org} burial rates over time and corresponding examples for proxies in the geological record. Values for the total organic carbon (TOC) content in organic-rich sediments, the normalized seawater $^{87}Sr/^{86}Sr$, and the average $\delta^{34}S$ of sulfate were adapted from Och et al[2], with permission from Elsevier. Increases in the latter two parameters indicate enhanced weathering fluxes. All rates were derived from our modeled scenario that include aerobic and anaerobic respiration and exclusive oxygenic photosynthesis. Shaded areas represent the range of rates dependent on 1.5–3.7% modern oceanic coverage by benthic coastal mats (corresponding to 20–50% of global marine C_{org} burial during the mid-Proterozoic) and a continental coverage of 5% by terrestrial mats. Changes in global coastal benthic and terrestrial C_{org} burial fluxes are driven by changes in daylength and are shaped by feedback effects of increasing pO_2 (Fig. 4) on aerobic respiration. Pelagic burial, atmospheric reduction by volcanism- and metamorphism-derived gases and weathering were parameterized for a reference pO_2 of 0.1 in the mid-Proterozoic[60]. The rate of atmospheric reduction was assumed to be constant and determined by the flux of reduced gases. In contrast, the rate of erosional weathering increases with daylength as it depends on pO_2 and C_{org} burial by terrestrial mats.